NTNU

Norwegian University of
Science and Technology

Load measurements at riprap toe.

Kofi Ntow Opare

Hydropower Development
Submission date: June 2018
Supervisor: Fjola Gudrun Sigtryggsdottir, IBM
Co-supervisor: Ganesh Hiriyanna Rao Ravindra, IBM

Norwegian University of Science and Technology
Department of Civil and Environmental Engineering

Kofi Ntow Opare

Load Measurements at Riprap Toe

Master's Thesis in Hydropower Development

Trondheim, June 2018

Supervisor: Associate Professor Fjola Gudrun Sigtryggsdottir

Co-supervisor: Ganesh H.R. Ravindra.

Norwegian University of Science and Technology
Faculty of Engineering Science and Technology
Department of Civil and Environmental Engineering

Load Measurement at Riprap Toe.

ABSTRACT

Riprap is widely used as slope protection and when placed on the downstream slope of a rockfill dam, it provides erosion resistance under overflow conditions. For steep downstream slopes (S > 50%), initiation of riprap failure at the dam toe can be considered a possibility under overtopping conditions of rockfill dams. The present study focuses on the load generation mechanisms that are present at the dam toe in the event of overtopping. Placed ripraps for the tests were constructed in an interlocking pattern on a model of a downstream slope of an embankment dam in the hydraulic laboratory at NTNU, Trondheim.

In order to quantify the loads acting at the dam toe during overtopping, load cells were installed at the toe to measure those loads. Monitoring of load generation at the toe showed two different types of loads acting on the toe section of the dam. The first is the self-weight of the riprap stones during building of the riprap structure and the other is the hydraulic load as a result of overtopping of the dam. The effect of the latter at the toe is dependent on the discharge of the overflow with higher discharges resulting in higher hydraulic loads at the dam toe. The hydraulic load causes a two dimensional displacement of the riprap stones that causes the entire structure to deform in a buckling-like pattern resembling that of a slender long column pinned at one end and free at the other end. This buckling eventually leads to riprap failure. Rearrangement of the riprap stones resulted in progressive displacement of the stones along the slope leading to compaction of the stones at the toe section due to the fact that the entire structure is supported at the base and further loosening of the stones in the upper section. This compaction leads to a change in the magnitude of the effect of the riprap self-weight felt at the toe of the dam even when overtopping ceases.

ACKNOWLEDGEMENT

My first and foremost acknowledgement goes to the Almighty God for the gift of life and His abundant grace upon my life for it is He who works in me both to will and to do for His good pleasure (Philippians 2:13).

As a child, I had always been encouraged by my family to strive to achieve excellence in whatever I do. I would like to thank them my parents and siblings for their financial, spiritual and emotional support throughout my entire studies here in NTNU. Though far away from me, your support over the years has been overwhelming and I deeply appreciate it.

The help of the entire faculty in the Hydropower Development program is also appreciated especially my main supervisor Associate Professor Fjola Gudrun Sigtryggsdottir for her support throughout the course of this project. Also to my co-supervisor PhD candidate Ganesh Ravindra I would want to say a big thank you for your support through the lab sessions and all the great times we have had together throughout this project.

Finally the efforts of all friends here and abroad who have contributed in diverse ways in making this project a success is deeply appreciated. Special mention goes to the entire HPD 2016-2018 year group for the great atmosphere you created both in and out of the lecture rooms. Trondheim felt like home for some of us with you around. Thanks guys and wishing you well in all your future endeavors.

Contents

LIST OF FIGURES

LIST OF TABLES

1.0 INTRODUCTION

1.1 Background

Water is one of the most important commodities known to man. But over the years in some places, water has always not been available when it is needed and where it is needed. Dams and reservoirs have been built since time immemorial to help solve the problem of time variability of water. Over the years, dams have helped store runoff waters for use during drier periods of the year among many other important benefits. Of all the many advantages of dams, these massive structures are also very delicate structures whose failure when not properly built or managed can lead to a catastrophe. There has been a number of these catastrophic dam failure events in the past which have led to loss of lives and properties. These catastrophes include the Malpasset dam failure in France and the all famous 1963 Vaiont dam failure in Italy which resulted in approximately 2600 fatalities (Williamson, 2017).

Climate change which is causing extreme weather events like droughts, hurricanes, heat waves, floods etc. has called for much attention for structures built across water ways like dams most importantly embankment dams which are very vulnerable to extreme flood events. This is because when flood levels exceed the spillways capacities of these type of dams, it will lead to accidental overtopping of the dam core or even the dam crest. Since these dams are built with natural materials which are pervious and erodible, an accidental overtopping of these dams can lead to erosion of the dam material which may eventually lead to a dam breach. A dam breach will in turn lead to massive loss of lives and properties especially if it is situated close to densely populated areas.

Statistics from the International Commission on Large Dams (ICOLD) put overtopping as the number one cause of failure in earth dams accounting for 31% of the total cases recorded (ICOLD, 1995). This has led to a significant increment in social demand on dam safety standards especially in the most developed countries including here in Norway (Moran, 2015; G. Ravindra et al., 2018a). Norway at present has more than 185 large rockfill dams (dams of height 15 meters or greater). These dams often impound water creating behind them reservoirs of varying sizes used mainly for hydropower production. The Norwegian Water and Energy Directorate (NVE) gives regulations on the minimum safety requirements of these dams. One of such regulation is protecting the downstream slope of all embankment dams with stone riprap which is one of the

most common and cost effective measure for erosion, structural stability and slope stabilization (Hiller et al., 2017; G. Ravindra et al., 2018a).

Riprap is formed of rockfill or other natural materials used to armor shorelines, streambeds, bridge abutments, pilings and other hydraulic structures against scour and water or ice erosion. Provided on the upstream or downstream slope of an embankment dam, ripraps can serve different purposes. On the upstream face of an embankment dam, ripraps resist wave actions or currents from the reservoir which can cause erosion of the embankment material. On the downstream slope of the embankment, the primary function of the riprap is to provide erosion control of the downstream face of the dam under throughflow and or accidental overtopping situations as depicted in Figure 1 below. The elements forming the riprap can be randomly dumped on the slope surface or carefully placed one after the other to create an interlocking pattern which makes the riprap behave like a structural unit (slab) over the slope surface (G. Ravindra et al., 2018a).

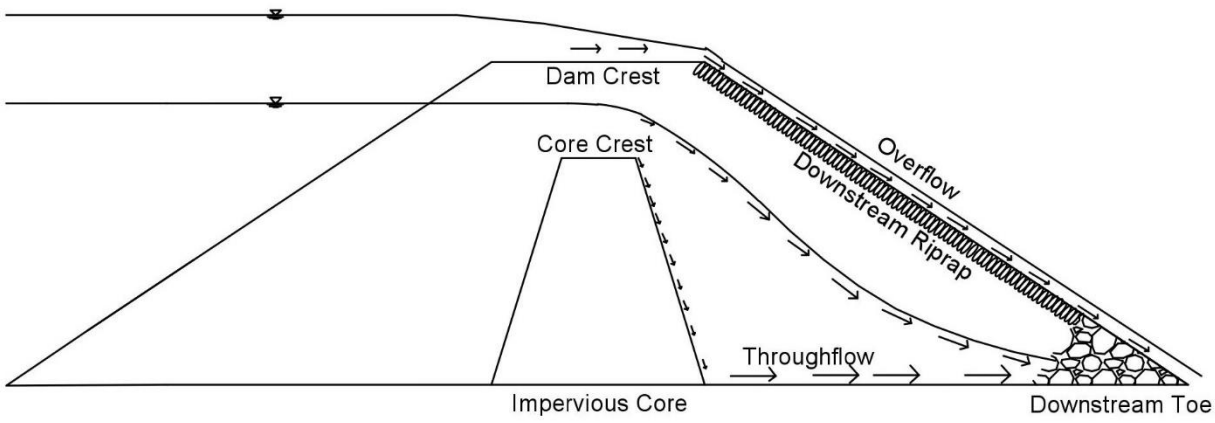

Figure 1 Illustration of flow concentration at the toe of an embankment dam under overflow and or throughflow scenarios

There has been extensive investigations into dumped riprap stability in the past but not much research has been conducted on placed riprap. But the very few research that have been conducted to understand the stability of placed riprap under extreme loading conditions has suggested that placed ripraps are able to withstand discharges 5 to 10 times that of dumped ripraps before collapse (Hiller et al., 2017). But the careful placement of stones in interlocking pattern in placed ripraps means that it requires more stones and also very skilled labor and sophisticated equipment compared to dumped riprap. Some of these investigations have also looked into the stability of embankment dams with steep downstream slopes (S > 50%) under overtopping situations and

found out that the probability of initiation of failure at the toe of the embankment can be very significant. This is because under overflow conditions, the toe of the embankment is inundated with highly turbulent flow which results in the generation of dynamic forces within the dam toe.

Figure 2 Laboratory model test which shows highly turbulent flow condition at the riprap toe on the downstream slope of an embankment dam. Photo by K.N. Opare

Due to the very turbulent flow conditions that give rise to these dynamic loads at the dam toe, quantification of these loads are very challenging. The dam toe has to deal with these dynamic forces that are transferred from the riprap unto it. This process can result in loosening of the riprap stones at the embankment toe which can results in removal of these stones which will in turn lead to a progressive collapse of the entire riprap structure. This situation is exacerbated if the downstream slope is steep ($S > 0.5$). Hence arriving at a qualitative and quantitative descriptions of the dynamic load generation mechanisms and finding ways to measure and quantify such loads at the toe of ripraps under overtopping conditions is of great importance as this can be of relevance for design of embankment dam toe structures.

1.2 Research Objectives

This background has necessitated the need for additional research into understanding the dynamic load generation mechanism at the toe section of riprap on the downstream slope of embankment

dams. Knowledge of this, will help in formulating a design criteria not only for sizing riprap toe stones like have been done in the past, but it will also help in assessing in much detail the failure mechanisms in riprap and coming up with criteria for the design of such sections of ripraps.

This study is therefore composed of a number of tasks in addressing the issue of load generation mechanisms in the riprap toe. The hydraulic laboratory in NTNU has a physical model of a steep downstream slope of an embankment dam on which several investigations have been made in the past. The main objective of this study therefore is to carry out additional investigations on this existing physical model in order to study the dynamic load generation mechanism at riprap toe section under overtopping conditions. Findings from this research should contribute to the process of developing a methodology for design of embankment dam toe structures if not come up with a design criteria for riprap toe section. This should also help in the general improvement in the safety of embankment dams. The specific tasks of the thesis is as detailed below:

1. Carrying out a literature review into the state of the art in riprap research and hydraulic load measurements pertinent to ripraps under overtopping conditions.
2. Planning of physical model investigations on the existing physical model in the hydraulics laboratory in the Department of Civil and Environmental Engineering here in NTNU to study the loading mechanism at riprap toe section. This includes preparatory investigations such as measurement of riprap stone sizes and weights.
3. Performing a number of overtopping tests on placed ripraps and documenting the measurements.
4. Analysis of the recorded load and riprap stone displacement data sets and evaluation of results.

1.3 Thesis Outline

This thesis is outlined to tackle the various tasks given in the objectives above. The first chapter which is introduction gives a background to the problem at hand and brief overview of the entire situation and clearly spells out the specific tasks of this thesis. From this introduction, the specific tasks are then tackled with chapter two made up of a literature review of relevant research on the topic that has been done in the past. Key findings from these investigations are summarized and referred to later in subsequent chapters of this work. The research methodology is described in the

chapter that follows including a presentation on the research instrumentation and also the physical overtopping tests. The results of the overtopping tests is then presented in the subsequent chapters with clear analysis of these results comparing them to previous findings and clearly showing new findings. In the final chapter, a conclusion of the entire work and recommended areas for further research in the future are given. Data from all the tests are also presented in the appendices.

2.0 LITERATURE REVIEW

In this section, riprap as slope protection structure is discussed in general. The two known types (dumped and placed) are also discussed with specific interest on parameters that influence the design of these ripraps and their failure mechanisms. Special emphasis is also laid on the toe section of the riprap as to the extent of research done in that section of the riprap. Then finally the chapter concludes with a look at load measurements in general with specific emphasis on hydraulic structures like riprap.

2.1 Riprap as Slope Protection

Runoff and potential additional loads on the downstream slope and crest of embankment dams require that these places be well secured. On the upstream side, erosion protection is also required to counter the action of wear from waves, ice action and altering water levels. From the early 1960s when many major dam projects were embarked on, there has been significant amount of research to optimize dam design to achieve more durable structures. The measures against erosion of accidental leakage or overtopping are divided into soft protections such as overtopping-resistant dumped or placed riprap and hard protections such as concrete slabs, shaped blocks or articulated concrete blocks according to Toledo et al. (2015). On the soft protections, research has proven that protecting the slopes of embankment dams with stone riprap is a cost effective measure for erosion, structural stability and stabilization (Hiller et al., 2017; G. Ravindra et al., 2018a).

2.1.1 Riprap Parameters

The stability of every riprap depends on the interaction between the riprap and the hydraulic forces acting on it. These parameters can be subdivided into riprap properties, hydraulic properties and the geometric boundary conditions (slope *S*, chute length L_s and width of channel *B*) (Hiller et al., 2017).

The riprap properties are often characterized through the riprap stone size which is expressed through either the stone diameter *d*, volume V_s or mass m_s. These parameters are related to each other through the expression:

$$V_s = C_f d^3 = C_f m_s \rho_s^{-1} \quad (1)$$

where ρ_s which is the stone density and C_f which is the form factor varying between 0.4 and 0.8

for schistose and cuboid stones respectively (NVE, 2012). The diameter is often expressed as the nominal diameter $d = (abc)^{1/3}$ (Bunte and Abt, 2001). Where a, b, and c represent the longest, intermediate and shortest stone axes respectively.

Particle size distribution curves also help describe the grading of the riprap stones. A common grading indicator is the coefficient of uniformity $C_u = d_{60}/d_{10}$. Abt et al. (2008) also found out that the shape of the riprap stones influence the stability. The finding showed that rounded stones need to be approximately 40% larger than angular stones to withstand similar flow conditions.

Hiller et al. (2017) further suggested that the way and manner that riprap stones are constructed further induces some properties such as packing density and riprap layer thickness. For placed riprap, an additional property which is the stone orientation can be described by the angle of inclination β between the chute surface and the longest axis of the riprap stone. From the packing density then came the packing factor:

$$P_c = 1/Nd_s^2 \quad (2)$$

where N is the number of stones per square meter area and d_s is the nominal diameter (Linford and Saunders, 1967). A low packing factor P_c indicates high packing density and vice versa. Tests from Hiller et al. (2017) showed that placed ripraps have lower P_c compared to dumped riprap and this made placed riprap withstand higher discharges compared to dumped riprap.

With regards to the hydraulic properties, the flow velocity v is the key parameter to describe the hydraulic forces such as drag, lift and shear. The flow over riprap is driven by gravity and mainly characterized by the Froude number $F = v(gh)^{-0.5}$, the Reynolds number $R = vhv^{-1}$ and Weber number $W = \rho_w h v^2 \sigma^{-1}$, with the acceleration due to gravity g, water level h, kinematic viscosity v, density of water ρ_w and surface tension σ. The Reynolds number can be ignored if the flow in the model and the prototype is turbulent. The Weber number is relevant to describe the transport of air. For high-speed air – water flow scaled with Froude similitude, Pfister and Chanson (2012) recommend $W^{0.5}$ greater than 140 or R greater than 2 to 3 * 10^5 to prevent significant scale effects (Hiller et al., 2017).

Hiller et al. (2017) further states that the Froude number F can be combined with the relative submergence hd^{-1} to the stone-related Froude number:

$$F_s = q(gd^3)^{-0.5} \quad (3)$$

With the discharge per unit width $q = vh$. For ease of comparing results from different scales, the use of F_s is recommended instead of F. The shortfall to this is that the determination of v and h is often close to impossible in supercritical flow due to unstable water depth and also the flow being highly aerated. But their product q remains constant as long as the geometry does not change. At failure and with the critical unit discharge q_c, the stone related Froude number becomes:

$$F_{s,c} = q_c/(gd^3)^{0.5}. \quad (4)$$

This parameter $F_{s,c}$ has traditionally been used to describe stability of ripraps (Hiller et al., 2017).

2.1.2 Riprap Failure Mechanisms

Riprap exposed to overtopping are characterized by different failure mechanisms. The possible failure scenarios for riprap include and are not limited to erosion of single stones, sliding of the protection layer and disruption of the protection layer (mainly due to lifting forces) as depicted in Figure 3 (Siebel, 2007).

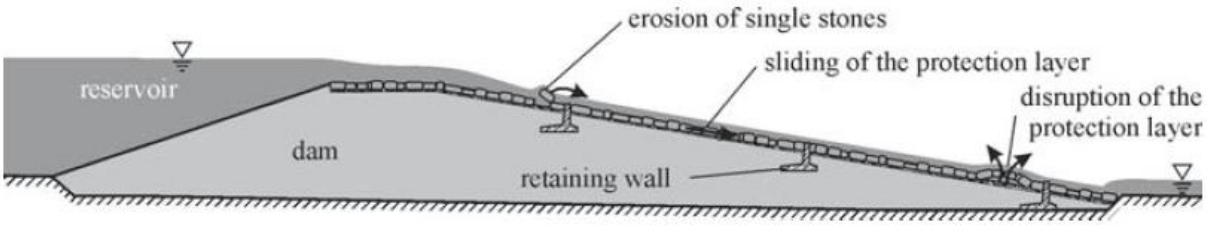

Figure 3 Possible failure scenarios of protection layers on overtoppable earthdams as depicted by Siebel 2007.

Failure of dumped riprap is usually achieved when there have been sufficient erosion of the riprap stones to expose the underlying filter layer (eg Linford and Saunders (1967); Siebel (2007)). Placed riprap on the other hand is made up of a single layer of riprap stones placed in an interlocking pattern. The interlocking nature of the riprap makes the riprap layer form a bearing structure capable of carrying or resisting some loads (Hiller et al., 2017; G. Ravindra et al., 2018a; Siebel, 2007). This property of placed riprap makes it behave differently from dumped riprap when it comes to the failure mechanism and also causes it not to fail as in dumped riprap when there is erosion of one single element that leads to exposure of the filter layer (Dornack, 2001; Siebel, 2007; Sommer, 1997).

The failure mechanism in placed riprap is sliding or rupture of the riprap layer (Dornack, 2001; Siebel, 2007; Sommer, 1997). Sommer (1997) conducted some tests and documented the rearrangement of stones resulting in displacements and compaction in the downstream part of the riprap layer and a loosening of the upstream part. The finding further suggested that bulk failure may be initiated due to the flow attack of the exposed stones in the loosened part of the riprap.

Hiller et al. (2017) conducted some tests and further suggested displacement as the leading cause of failure in placed riprap. The finding also showed that failure is normally initiated at the upper part of the riprap close to the crest where there is a loosening of the riprap as indicated by Dornack (2001). Based on the findings of Hiller et al. (2017), G. Ravindra et al. (2018a) further conducted tests where stone displacement was checked in a 2D way. The outcome of the test was that placed ripraps on steep slopes exposed to overtopping flows underwent a 2D buckling process resembling the buckling modes of a slender long column under compression pinned at one end and free at the other end (G. Ravindra et al., 2018a).

2.2 Riprap Design at Embankment Dam Toe

There has not been much investigations into the design of ripraps at the toe section of embankment dams with most of these investigations conducted in the past. In recent years, there has been few studies into this subject matter some of which are Moran, (2015) and Moran and Toledo, (2011) where their findings suggested that the toe section of embankment dams could be used as an effective protection for such dams against throughflow caused by either overtopping or a high leakage through the impervious core of the dam.

Solvik (1991) came up with a design chart for sizing what he termed keystones. Keystones are the last row of stones at the toe of the embankment dam. He opined that the stones are very crucial to the stability of the entire riprap on the downstream slope of the embankment and hence their removal will cause a total collapse of the riprap. His chart was developed from physical modelling studies conducted to study problems in rockfill dams exposed to exceptional loads. The chart was also used in sizing the so called keystones in dumped riprap. The chart does not give any sizing criteria for placed riprap and was developed solely on the basis of the importance of these keystones but not necessarily on the basis of the magnitude of the exceptional loads that these stones are exposed to.

Similar to Solvik's findings (with regards to dumped riprap), Abt et al. (1998) conducted experiments on a pilot flume where flow overtopped an embankment with a mild side slope S = 20%. The flow then went over a toe structure made of 90, 130 and 200mm as median stones. Their investigation focused on two sections of which are the side slope and the toe sections. They recorded critical flow values that caused movements in stones at the two sections and realized that stones at the toe required less critical discharge values as compared to their counterparts at the side slope section as shown in Table 1.

Table 1 Experimental test results from Abt et al., (1998). a Median stone size (mm); b Unit discharge for riprap stone movement at the side slope; c Unit discharge at toe stone movement.

(D_{50})[a] (mm)	**(qRR)[b] (m3/s/m)**	**(qT)[c] (m3/s/m)**
200	0.54	0.26
130	0.36	0.09
90	0.26	0.08

Their investigation further proved that for a riprap, toe stones should be approximately twice the size of the stones in the side slope (Abt et al., 1998). They further developed a criterion for sizing toe stones of dumped ripraps with the slope and the unit discharge as parameters.

$$D_{50(min)},\ T = S^{0.43}(C_f q_f)^{0.56} \qquad (5)$$

Where, D_{50} is the minimum required median stone at the toe (*mm*), *S* is denoting the design slope in percentage, q_f being the design critical unit discharge, C_f is a flow concentration coefficient dealing with uniformity of the graded slope as a result of flow channelization.

There have been recent findings on the downstream slope protection on embankments. Ravindra et al. (2018) compiled findings from some of these different performance-based evaluations on dumped riprap sizing criteria. The review shows that the Thornton et al. (2014) and the Khan and Ahmad (2011) approaches for sizing dumped riprap stones best predicted the physical modelling test results obtained from some of the numerous past investigations. Out of the two approaches, the Thornton et al. (2014) approach is viewed as being marginally better compared to the approach

from Khan and Ahmad (2011) (G. H. R. Ravindra et al., 2018). The review further proposed a modified sizing equation based on the equations from these two findings.

$$D_{50}, T = K\, t^a\, S^b\, C_u^{\,c}\, (C_c q_f)^d (SG)^e \qquad (6)$$

Where t is the thickness of the riprap layer, S is the design slope, C_u is the coefficient of uniformity (D_{60}/D_{10}), C_c is the coefficient of concentration, q_f is the design critical unit discharge and SG is the specific gravity of the construction material.

As can be inferred from the equation, toe stone sizing could be primarily influenced by thickness of the riprap layer, side slope of the downstream embankment, particle size distribution, design unit discharge and properties of material employed for construction and shape of abutments (G. H. R. Ravindra et al., 2018).

2.3 Load Measurements

There has not been much investigations into load measurements on riprap layers let alone the toe section of the riprap. Siebel (2007) investigated the reaction that hydraulic loads cause on riprap layer which induces failure of the layer through erosion of single stones, sliding of the protection layer and disruption of protection layer as depicted in Figure 3. The investigation adopted different test setups to investigate these three different failure mechanisms.

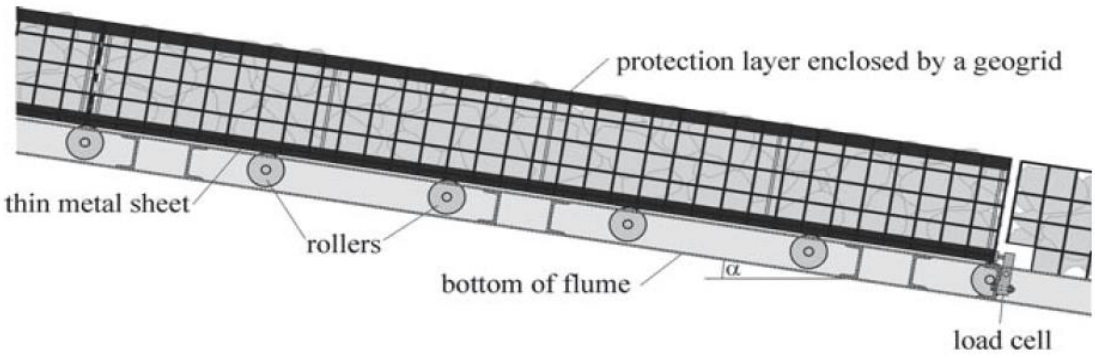

Figure 4 Siebel 2007's illustration of slope protection layer on rollers with attached load cells for the experiment on sliding.

For the experimental setup used for the sliding tests, a flume was equipped with a multitude of rollers in the bottom with a riprap layer enclosed in a geogrid placed on a thin metal sheet applied to these rollers almost without any friction as described by Siebel (2007). Two load cells were

installed in the bottom end of the flume as shown in Figure 4 to prevent the protection layer from rolling down and also help measure the forces acting parallel to the slope of the setup.

3.0 EXPERIMENTAL SETUP AND PROCEDURE

3.1 Research Instrumentation and Setup

The model riprap constructed in the 25m long, 1m wide and 2m high flume in the hydraulic laboratory at NTNU is used in this experiment. Slight modifications are effected to the model compared to the one used by Hiller et al. (2017) to make way for the installation of load measurement devices at the toe of the riprap. Hiller et al. (2017) gives a detailed description of the experimental instrumentation and procedure. For ease of referencing, an overview of the instrumentation and the procedure with specific emphasis on the modifications that have been done to the model for this experiment are presented here.

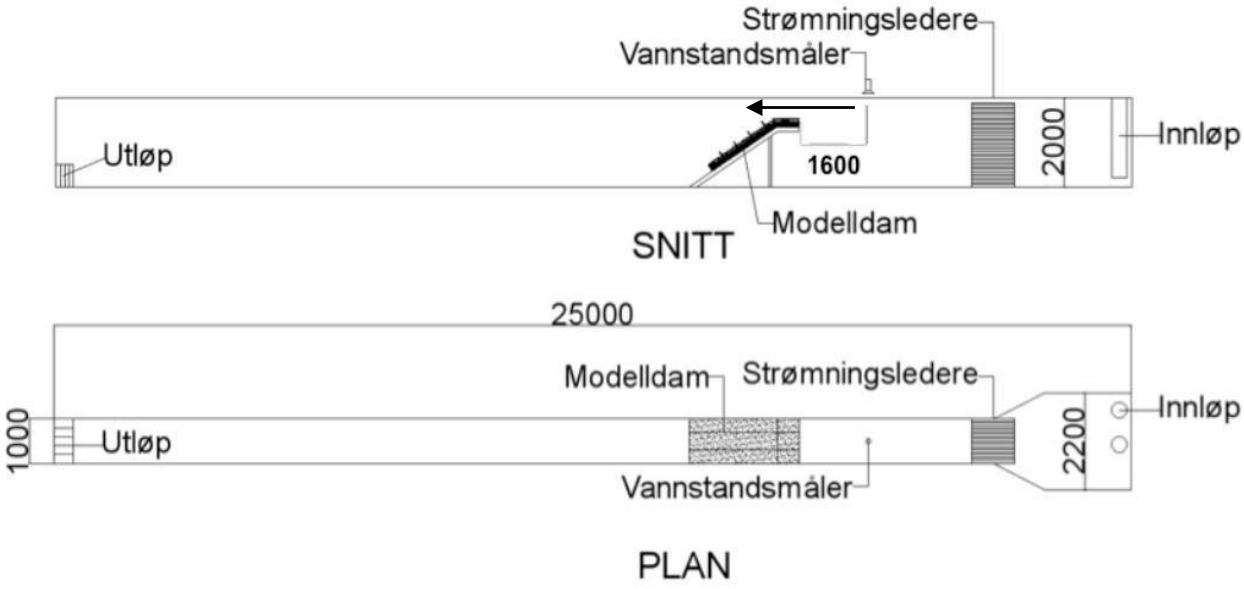

Figure 5 General plan and section of the test flume in the hydraulics laboratory at NTNU as illustrated by (Pattersen,2015).

Hiller et al. (2017) designed and tested a conceptual 1:10 model consisting of a single layered placed riprap section of width 1m and total chute length L_s = 1.8m constructed over a base frame inclined at 1:1.5 (S = 0.67) as shown in Figure 6.

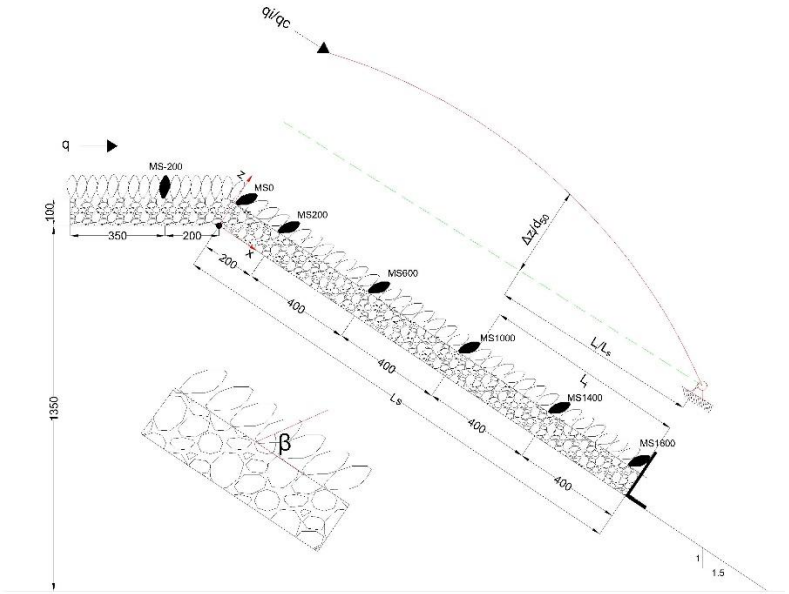

Figure 6 Test set-up for experiments with placed riprap as used by (Hiller et. al., 2017)

The total chute length L_s has been reduced to 1.75m to make way for the installation of the load cells which will help in measuring the loading situation at the toe of the riprap during construction and also during the overtopping tests. This modification is also shown in the Figure 7.

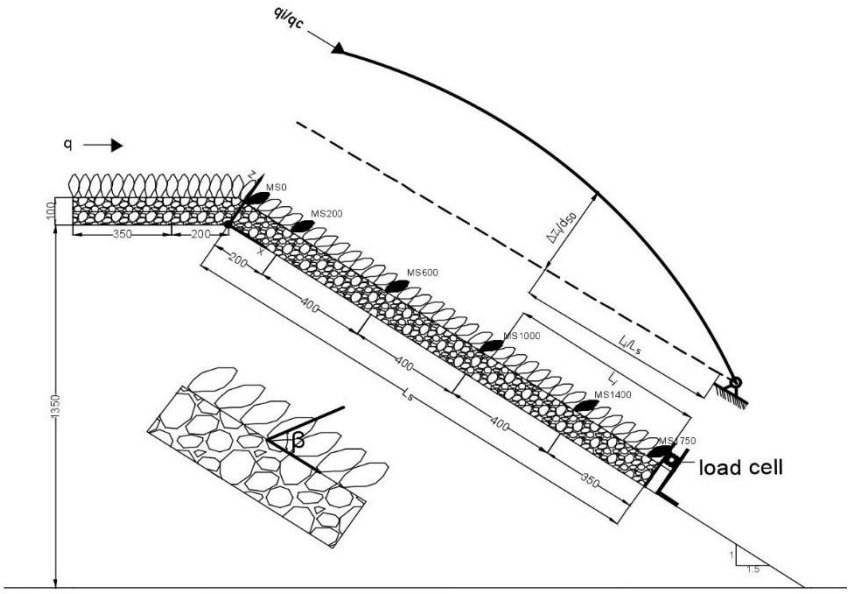

Figure 7 Modified test set-up with load cells incorporated at the riprap base and a shortened chute length from 1800mm to 1750mm used for this current experiment.

The ripraps were supported at the toe with three metallic support structures which sit on six load cells (two load cells per metallic structure). The entire setup was elevated from the flume bottom to avoid backwater effects at the toe during the overtopping tests. The setup was also situatuated sufficiently downstream of the inflow section to achieve a calm flow as it approaches the riprap crest. Discharge to the flume was provided by pumps with combined capacity of 0.4 m^2/s. An automated 3D-traverse system coupled with a laser displacement meter was used to measure the displacements of the riprap stones after every discharge during the overtopping tests. The system measured the location coordinates of selected riprap stones in Cartesian coordinate system with its origin situated at the transition from the horizontal crest to the inclined chute as shown in Figure 6. The *x*-axis was aligned in a direction parallel to the chute (33.7^o to the flume bottom) and the *z*-axis was set perpendicular to the chute. Location coordinates could be measured to an accuracy of 0.1mm in the x-direction and 1mm in the z-direction. Stone displacements were considered only along the *x* and *z*-directions as any possibility of lateral flows resulting in stone displacements in the y-direction was ruled out.

3.1.1 Load Measuring Device / Force Transducer (S9M/500N)

The S9M/500N force transducer is a device manufactured by HBM. The S-shaped S9M load cells measures tensile and compressive forces and can be used for various kinds of static and dynamic applications. The S9M is tailor made to suit difficult applications in that the measuring body is made of stainless steel and is well welded which makes it an ideal option for this kind of test. Installed at the riprap toe during overtopping tests meant that the device was soaked in water during testing and hence its ability to work in such conditions without affecting the outcome of the results was very good. The S9M has nominal (rated) forces ranging from 500N to 50kN. Six (6) of the 500N load cells were used for this experiment giving it a combined capacity of 3kN.

Figure 8 The S9M load cells used for the experiments.

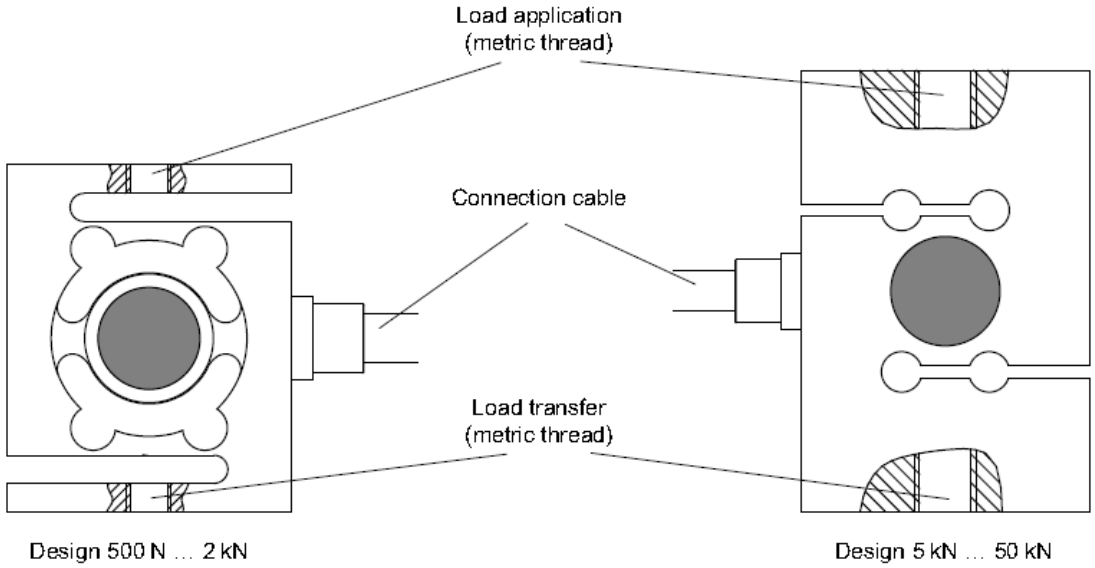

Figure 9 Sketch showing the various components of the load cell for the various nominal rates as depicted by HBM.

The S-shaped S9M load cell works in similar principle as a strain gauge because it has a strain gauge inside it. Strain gauge is an electrical conductor firmly attached to a film in a meandering pattern. When the film is pulled, the conductors get longer and when contracted, they get shorter. This results in a change in resistance of the conductors and the strain is determined on the basis of this because resistance grows when there is strain and diminishes when there is contraction. In the case of this force transducer, the electrical conductors of the strain gauge are securely bonded onto a spring element. This spring element is either elongated or contracted under the influence of force. The force transducer contains four strain gauges connected in a ring in a Wheatstone bridge circuit. The strain gauges are firmly attached to the steel of the transducer and therefore undergoes the same deformation as the strain gauge. When the steel is deformed, the resistance of the strain gauges change. The output signal from the bridge circuit then provides information on how great this deformation is. Then from that, we get the force acting on the strain gauges.

3.2 Experimental Procedure

3.2.1 Riprap preparation and measurements

The tests were carried out on a riprap layer which was overlaid on a filter material over the model of a downstream slope of an embankment dam in the hydraulics laboratory in NTNU as shown in the previous chapter. The filter medium was made up of 100mm thick layer of smaller stones and

a geotextile material placed over the chute of the slope. This according to Hiller et al. (2017) is in agreement with guidelines for the construction of embankment dams given by the Norwegian Water and Energy Directorate (NVE). The stones used for the riprap layer were the same used earlier by Hiller et al. (2017) which is mainly rhyolite obtained from a quarry.

New set of measurements were obtained from the riprap stones to help determine the nominal diameter of the stones. This was derived from the grain size distribution by mass of 500 of the riprap stones. The nominal diameter was then calculated from the formula $d_{50} = (abc)^{1/3}$ (Bunte and Abt, 2001) where a, b and c are the longest, intermediate and shortest axis of the stones respectively. The measurement was done with a handheld laboratory calipers. The stones were also weighed to determine their masses. Values obtained were compared to those from Hiller et al. (2017).

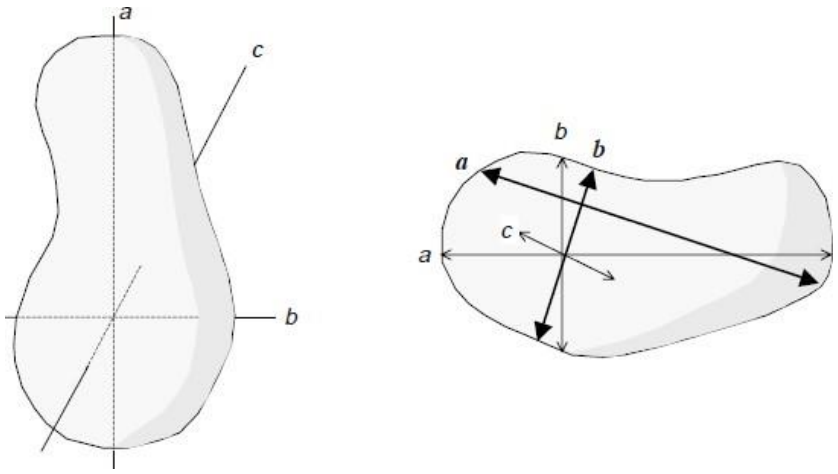

Figure 10 Illustration of stone axes from (Bunte and Abt, 2001).

3.2.2 Overtopping tests

Placed ripraps were constructed by manual placement of stones in an interlocking pattern commencing at the toe and progressing upstream to the crest. Load cell readings after placement of every fifty riprap stones were recorded and a curve generated afterwards to check the progress of the effect of riprap building at the toe. All test ripraps were constructed with a fixed chute length of 1.75 m requiring on the average 1100 stones. Riprap stones on the slope were deliberately placed with the longest axis (a-axis) inclined at an angle $\beta = 60^{o}$ with respect to the chute bottom and with an inclination $\beta = 90^{o}$ for stones placed on the horizontal crest to account for practical

considerations. This was so because the crest portion was not the point of focus of the experiment since that part is not considered as part of the downstream slope. Also the riprap stones used at this portion was slightly bigger and heavier than those used on the slope so that they become stable enough and not fail before the ones in the focus area which is the downstream slope.

Figure 11 Constructed riprap ready for overtopping test with marked stones at specified distance from the toe for observing displacements. View from both upstream and downstream. View from downstream also shows installed load cells. Photos by K.N. Opare.

Upon construction of the riprap, selected stones identified as MSxx in Figure 11, where 'xx' represents the x-coordinates of the stones were tagged with unique point markers and the previously described positioning system was used to measure the initial location coordinates (x,y,z) of these individual stones. The marked stones were located approximately along the centerline of the flume (y = 0.5 m) at specific positions of x = 0, 0.2, 0.6, 1.0, 1.4 and 1.75 m. With the entire setup ready for the overtopping tests, unit discharges (q_i) were supplied in step-wise increments of 0.025 m^2/s starting from q_i = 0.05 m^2/s until the critical discharge q_c where the riprap collapses. Each incremental discharge was allowed to overtop the riprap setup for a specific time interval Δt = 30 minutes. After each incremental discharge, the discharge over the riprap was stopped and the location coordinates of the marked stones were measured. This procedure was repeated until total failure of the riprap structure was achieved.

3.2.3. Overview of Tests

Overall the 10 tests conducted took 9 weeks to complete spanning from January 2018 to March 2018. This time included preparation of the model and measurements of riprap stones which was done in the first week of the testing period. The remaining 8 weeks were used for the 10 overtopping tests which included riprap building, marking of selected riprap stones, overtopping tests and stone displacement measurements and finally cleanup and preparing the setup for the next test. Preparation of the setup was done sometimes by one person or at times by two people but overtopping tests always required two persons. This was because overtopping tests required one person operating the laser scanner used to check the stone displacement which was fixed over the flume and the other person monitoring and recording these displacements. And this was to be done concurrently hence the need for two persons at a time.

The overview of the tests is given in the Table 2 with details given in subsequent chapters of this thesis. L_s stands for the chute length which was constant for all the tests, P_c for the various packing factors, q_i gives the range of the various incremental unit discharges for each test with n giving the number of incremental discharges obtained per test before riprap failure, Δt shows the time for that each incremental discharge was run and finally q_c the critical discharge which is the discharge for which the entire riprap failed.

Table 2 Summary of all overtopping tests

Test	**L_s (m)**	**P_c**	**q_i(m^2/s)**	***n***	**Δt (sec)**	**q_c (m^2/s)**
2	1.75	0.58	0.05 - 0.2	7	1800	0.2
3	1.75	0.56	0.05 - 0.275	9	1800	0.275
4	1.75	0.57	0.05 - 0.15	5	1800	0.15
5	1.75	0.56	0.05 - 0.2	7	1800	0.2
6	1.75	0.56	0.05 - 0.15	4	1800	0.15
7	1.75	0.53	0.05 - 0.175	6	1800	0.175
8	1.75	0.53	0.05 - 0.325	11	1800	0.325
9	1.75	0.56	0.05 - 0.2	7	1800	0.2
10	1.75	0.56	0.05 - 0.125	4	1800	0.125

4.0 RIPRAP STONE MEASUREMENTS

Measured parameters of 500 of the riprap stones were compared with values from Hiller et al. (2017). This is because the materials used in this study were the same used initially by Hiller et al. (2017). This was done to check if there had been any alterations in the riprap stone properties. The measured parameters compared in both studies are as shown in Table 3. The measured parameters for all 500 measured stones are presented in the appendix.

Table 3 Measured riprap stone parameters compared with values obtained from Hiller et. al. (2017)

Parameter	**Value measured**	**Value from Hiller et al.**
Average longest axis length, a (m)	0.088	0.091
Average intermediate axis length, b (m)	0.049	0.053
Average shortest axis length, c (m)	0.036	0.038
Average nominal diameter, $d_{50}=(abc)^{1/3}$ (m)	0.053	0.057
Average mass of stones (kg)	0.21	0.24

From Table 3, it is observed that values obtained compared to values from the previous study differ slightly with these current values being slightly lower in magnitude. There has been approximately 10% reduction in the measured parameters. In between these two studies, the riprap materials have been used for other different tests and hence have experienced some wearing. It is observed that the stones have altered some of their properties as described by Hiller et al. (2017). They are gradually losing their sharp edges to a smooth surface as seen from the values in the table where the average length in all the three axes are reduced and also the average mass of the stones.

The slight alteration in the parameters of the riprap stones especially the smooth edges of the riprap stones meant that the riprap structure fails at slightly lower discharges on the average compared to failure discharges from Hiller et al. (2017). More rounded riprap stones means that riprap stones should have been at least 40% larger than they were before to be able to withstand the same discharges as established by Abt et al. (2008).

5.0 RIPRAP BUILDING LOADS

5.1 Load Profile at Riprap Toe during Riprap Construction

With the load cells fixed at the toe of the model before riprap was built, the loading situation at the toe was monitored while the riprap was being built. To remove occasional flat lines in the load profile due to breaks within the building process, load profile was checked against the length along the chute of the slope instead of against time. After placing of every 50 riprap stones, the length covered on the chute was recorded and later plotted against the load recorded on the load cells for that particular number of stones.

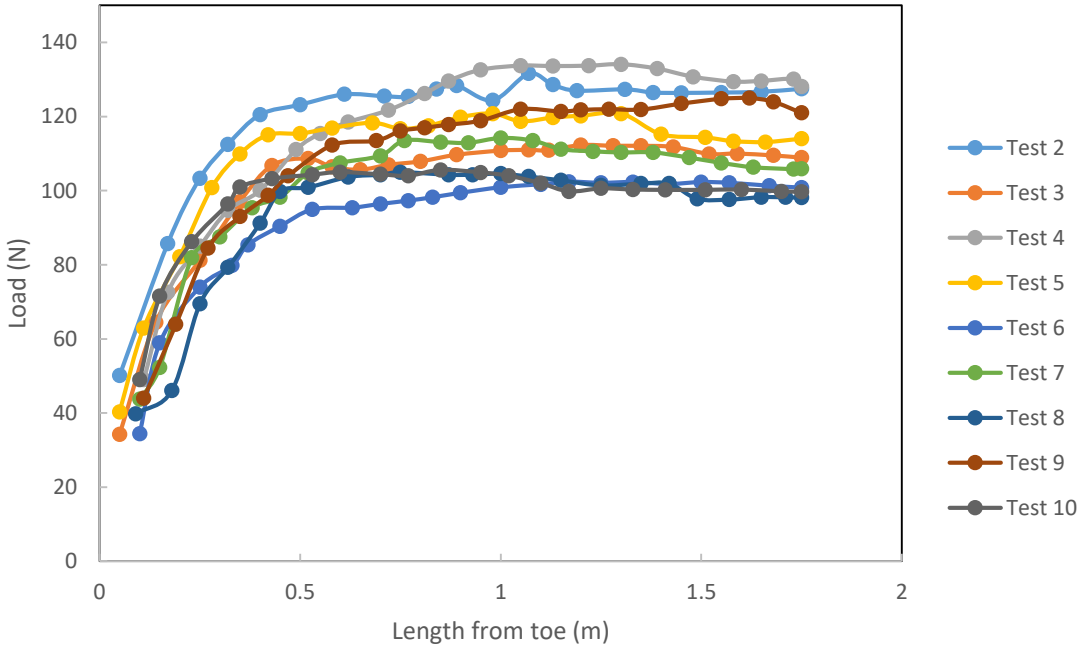

Figure 12 Progress of riprap stone self-weight on the dam toe as recorded during riprap construction for all tests. It is seen how the load stabilizes after a threshold distance from the toe.

Figure 12 shows the variations of the loads recorded at the riprap toe during construction for all the tests. It is observed that the load for lower third of the chute length, the load increases rapidly then gradually reduces through the middle third until it finally sort of stabilizes. From this point onwards, addition of more riprap stones cause no change in the load cell reading. Meaning the weight of the stones above a certain threshold length has no significant influence at the toe of the riprap. Beyond this threshold point, the weight of added riprap stones is carried by the underlying layer and the friction resistance from the underlying filter layer.

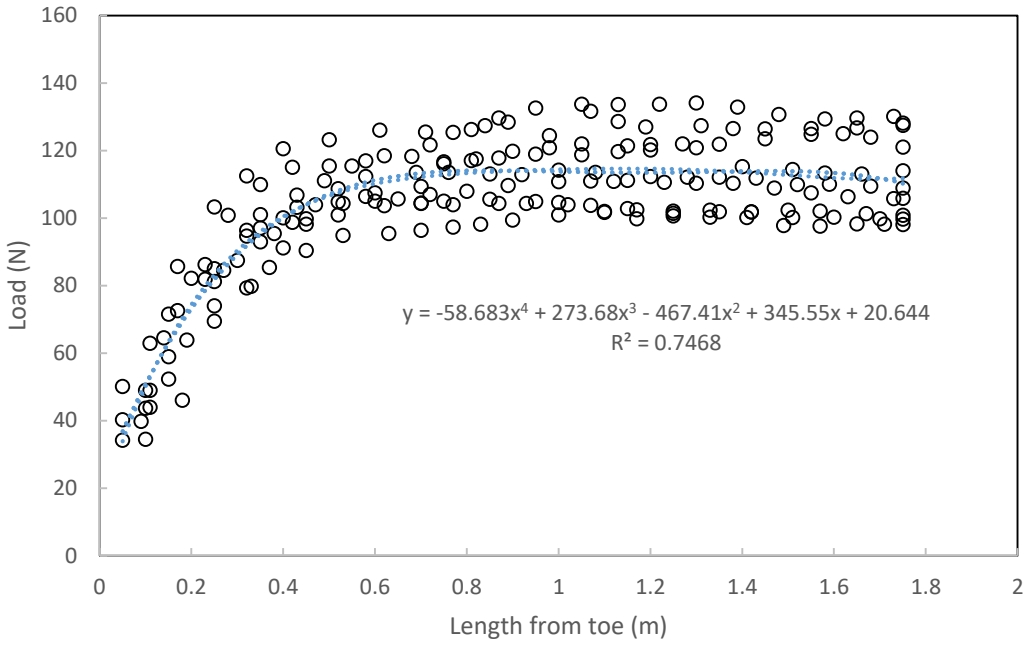

Figure 13 Scattered riprap building load profile for all tests to find the threshold distance at which the building load stabilizes.

To find the threshold length at which the load stabilizes, a scatter plot of all the tests is plotted as shown in Figure 13. A trend line that gives a good R^2 is fitted and the equation of the trend line given as shown in the figure. From the equation, different *x* values were chosen being the length from toe of the riprap to check the point at which the load stabilizes as given in table 4.

Table 4 Average load generated at every point along the chute of the riprap length which shown the threshold stabilization distance to be 0.7 m from the toe.

Length from toe (m)	Load (N)	Length from toe (m)	Load (N)
0.1	50.8	1.0	113.8
0.2	73.2	1.1	113.5
0.3	89.2	1.2	113.5
0.4	100.1	1.3	113.6
0.5	107.1	1.4	113.8
0.6	111.2	1.5	113.9
0.7	113.3	1.6	113.4
0.8	114.0	1.7	111.7
0.9	114.0	1.8	108.3

From Table 4 it is observed that the riprap weight measured at the toe of the riprap structure during construction of the riprap stabilizes at a distance of 0.7 meters from the toe of the embankment.

This distance is equivalent to 13.5 times the nominal diameter of the riprap stones. This means that stabilization occurred after about 14 rows of riprap stone placement. Any further stone placed beyond this distance did not have any significant effect at the toe of the embankment.

5.2 Load Resolutions at Riprap Toe

With tests showing that riprap building loads recorded on the cells at the toe of the riprap stabilizes at a distance of around 0.7 meters from the toe of the structure, that portion of the riprap has been isolated and the loading conditions analyzed to get a clear understanding of the forces at play within the riprap and the filter layer.

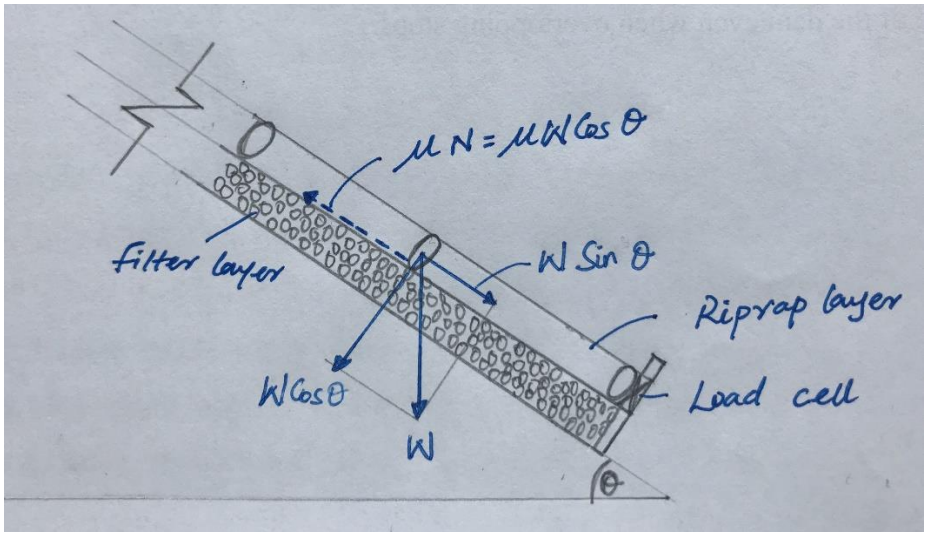

Figure 14 Force resolutions within a section of the riprap layer.

Taking a portion of the entire riprap section say the part which have influence on the load cell at the toe (0.7 m from the toe) and resolving forces to check if the load cell records the exact weight of the riprap stones resolved along the slope as depicted in the diagram above. From the packing factor, the approximate number of riprap stones within the specified length of the chute was calculated and multiplied by the average riprap stone mass as given in the previous chapter. This gives an indication of the mass of the riprap stones within this zone. The mass is multiplied by acceleration due to gravity to get the weight of the riprap (W) which acts downwards in the direction of gravity. The weight can now be resolved to $W\ Sin\ \theta$ which acts along the slope downwards and $W\ Cos\ \theta$ which acts perpendicular to the slope. Barring any friction, the reading on the load cell should be equivalent to the resolved weight in the direction along the slope of the incline which is $W\ Sin\ \theta$ but the average value of the load cell recorded value is approximately just

a quarter of the resolved weight along the slope. This is attributed to the friction from the underlying filter layer and the walls of the flume. Also the interlocking forces within the riprap means that not the entire weight of the riprap stones will act on the load cell. The full sliding resistance force which is given by $\mu WCos\theta$ is not mobilized because there is no acceleration of the stones. This is valid during riprap construction but during overtopping these stones are moved a bit but the friction resistance never gets fully mobilized.

6.0 OVERTOPPING TESTS RESULTS

Ten (10) overtopping tests were conducted and data sets and results obtained analyzed. Test one was used as a test trial so results from that test has not been included in this final analysis. For clarity and to avoid confusion, though results from test one has not been included, the subsequent tests maintained their original test numbers thus tests 2 through to 10. A brief summary of the nine tests is given in Table 3 while the detailed results from all these tests are provided in the appendices. L_s stands for the chute length which was constant for all the tests, P_c for the various packing factors, q_i gives the range of the various incremental unit discharges for each test with n giving the number of incremental discharges obtained per test before riprap failure, Δt shows the time for that each incremental discharge was run and finally q_c the critical discharge which is the discharge for which the entire riprap failed.

Hiller et al. (2017) suggested the packing factor to be a factor that determines the critical discharge of placed riprap, this study has found no clear relation between the packing factor and the critical discharge as shown in Figure 15.

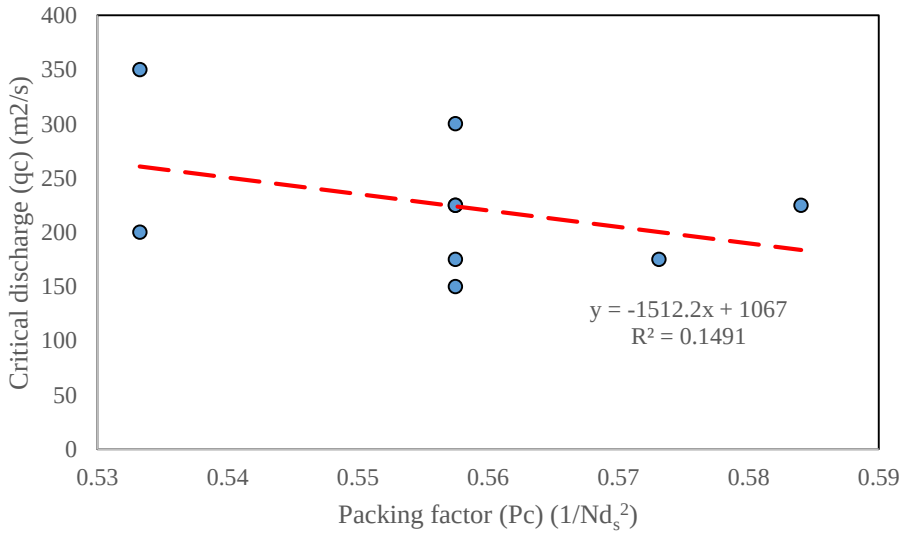

Figure 15 Graph of critical discharges against packing factors for all overtopping tests which shows no linear relation.

6.1 Load Profile at Riprap Toe

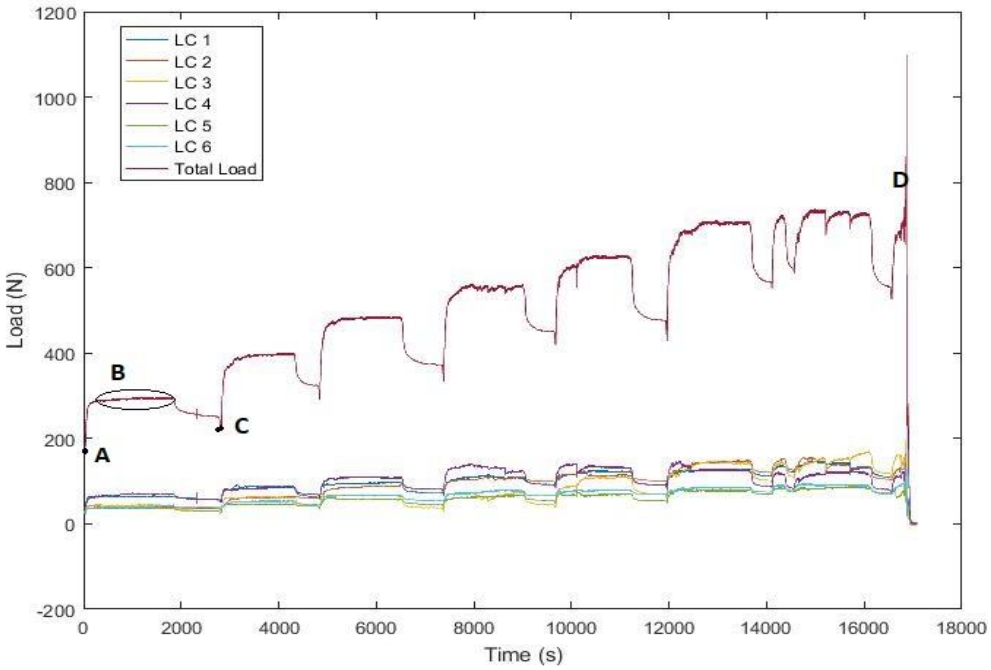

Figure 16 Typical load generation profile for an overtopping test obtained from the load cells with all six individual readings and then a summed up total reading for all the cells combined (Test 2).

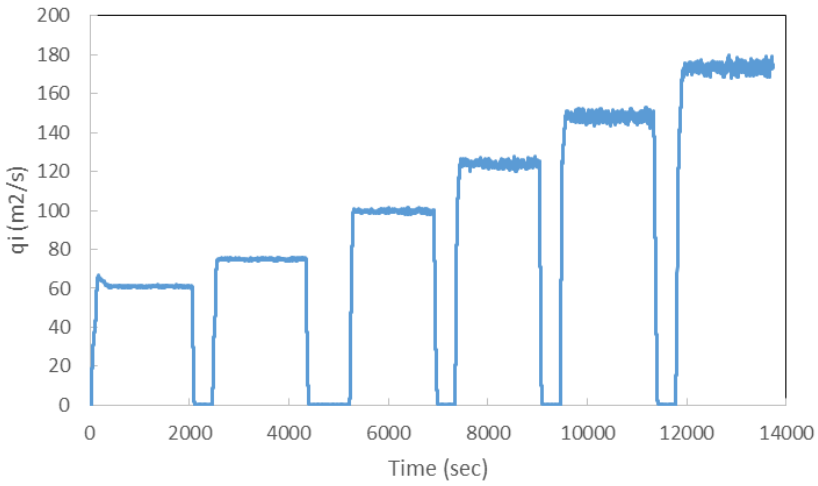

Figure 17 Typical discharge profile for the overtopping tests showing the incremental unit discharges and the gaps being shut down time for stone displacement measurements. (Test 9)

The general loading profile as recorded by the load cells installed at the riprap toe is as shown in Figure 16. Load is the reaction that the load cells measure. This presents the progression of the recorded load on all six of the load cells with time. A combined total load is also presented as seen

in Figure 16. The total load graph and data from it is used for all analysis because the interlocking forces within the riprap means that the readings registered by the individual load cells were not representative enough since the whole riprap acted as one structural unit placed on the filter. A critical look at the readings of the individual cells shows higher values recorded for the cells in the middle while the cells at the two ends of the riprap structure typically recorded lower values compared to their middle counterparts. At the onset of the overtopping test, the loading at the riprap toe is as a result of the weight of the riprap stones indicated on the figure as point *A* which has been discussed in the previous chapter. When the pumps are opened for the first incremental discharge, it overtops the riprap and unto the toe of the riprap which causes the load to rapidly increase till it gets to the region *B*. The discharge is left on for thirty minutes and once the loading reaches a certain limit, it either stabilizes, gradually increases or gradually increases for a while then stabilizes until the end of the thirty minutes when the pump is turned off then the load rapidly decreases to point *C*. Within the zone *B*, the maximum value is chosen as the total load from that incremental unit discharge (q_i). It is observed that point *C* has a higher value than point *A* which means that at shut down of the pump, the load does not return to the initial load before the overtopping. This means that the hydraulic loads from the overtopping water causes compaction of the riprap which results in permanent deformation. This completes one cycle of the test. At the shutdown of the pump after each cycle, the displacement of the marked stones are recorded with the laser scanner. The cycles were continued until total riprap failure was achieved as shown by the point *D*. It is worthy to note that at the onset of the overtopping and at lower unit discharges, flow over the riprap is highly aerated and turbulent then as the unit discharges increased through the cycles, the zone of aeration also moved gradually from the crest of the riprap towards the toe until at very high discharges, the entire chute is covered with non-aerated flow and a clearly defined water depth above the riprap is defined. At very high discharges, it was realized some distortions or noise in the load profile and this is attributed to the fact that at those discharges, there is occasional removal of individual stones from the riprap structure which rolls down the chute and hits the load cells causing a spike in the reading.

Figure 178 Two different overtopping scenarios during tests. Low discharge resulting in highly aerated flow over the entire riprap on the left and high discharge resulting in a complete clearly defined depth of water over the riprap layer on the right.

6.2 Riprap Failure

As opposed to dumped riprap, placed riprap does not necessarily fail when the underlying filter layer is exposed. Since placed riprap is made up of just a single layer of stone riprap, a removal of just one single stone will expose the filter layer which in the instance of dumped riprap would have been considered as failure. Instead, the interlocking pattern in which placed riprap is built makes it form a bearing structure which means that individual stones do not act on their own but rather the entire riprap work together as a unit and hence removal of a single stone does not cause failure of the entire riprap. Even though failure is not caused by the removal of one stone, this removal can result in a weakening of the riprap structure and change in the flow dynamics around the part where the stone is removed which can cause further removal of stones around that portion which can eventually result in collapse of the entire riprap.

During the overflow tests, riprap failure was considered when there was total collapse of the riprap or when there have been a considerable washing away of many riprap stones that it could clearly be seen that the integrity of the riprap had been compromised even though the structure was still standing. It was observed that during the tests, there were instances where loosely placed lone stones detached from the entire structure but the riprap structure worked perfectly.

Figure 18 Removal of a single stone after one of the overtopping tests. Entire riprap structure worked perfectly even with that stone removed.

Measuring the displacement of the 6 marked stones also showed that stones in the upper part of the chute underwent a bigger displacement compared to stones at the toe section of the riprap. As proved by Sommer (1997), this difference in displacements or rearrangement of the riprap stones causes compaction of the stones at the toe section of the riprap and also a loosening of the stones in the upper part of the chute which results in exposing the filter layer at the upper part of the riprap. Since a 2D displacement of the marked stones was recorded, these displacements were checked against the findings of G. Ravindra et al., (2018a) which suggests buckling as the cause of failure in placed riprap supported at the toe.

6.2.1 Buckling of Placed Riprap

G. Ravindra et al. (2018a) found that for a placed riprap supported at the toe like in the case of this experiment, overtopping makes the riprap behave like a slender long column pinned at one end and free at the other end which has been subjected to compressive forces. The Euler theory for column buckling which has been widely implemented in structural engineering was employed to describe the buckling observed in placed ripraps in the study. This study will not go into detail the structural engineering Euler theory but the observed displacements for the marked stones is compared with results from G. Ravindra et al. (2018a) and the buckling-like pattern as observed from the tests is given. It is worthy of note that even though the Euler theory is built for columns which are continuous structures, we compare marked displacements of stones placed in a line and interpolate linearly between these marked stones to see the pattern.

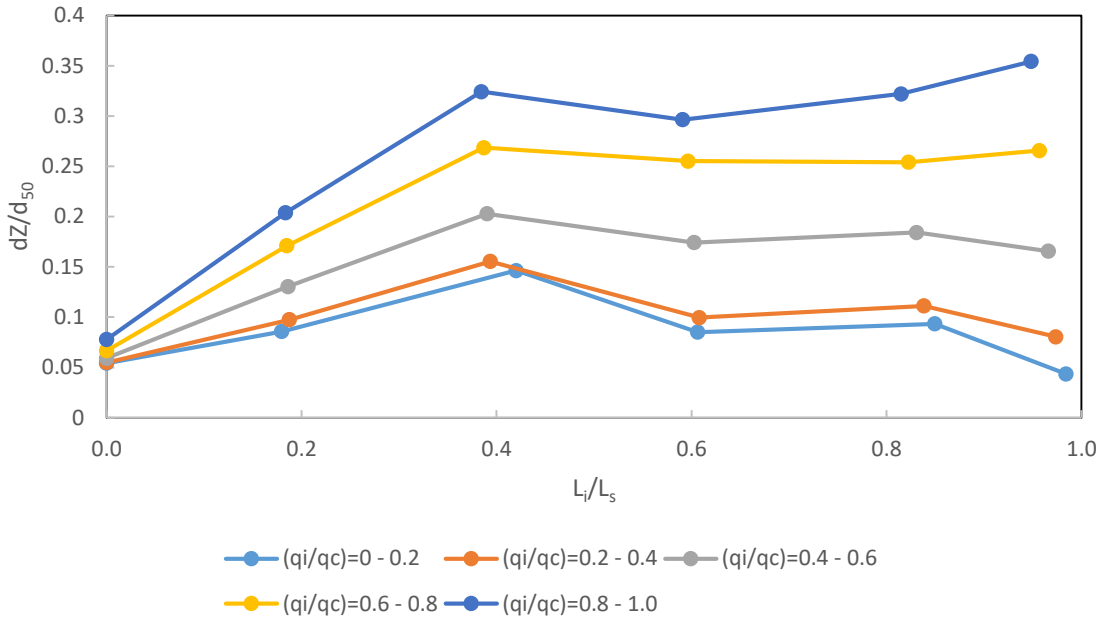

Figure 19 Observed 2D displacement of the six marked stones for showing buckling-like pattern of riprap for all tests combined.

For ease of comprehension for simplification, incremental discharges (q_i) for all the tests have been normalized with the critical discharge (q_c) for all the tests and categorized into five groups 0 – 0.2, 0.2 – 0.4, 0.4 – 0.6, 0.6 – 0.8 and 0.8 – 1.0. This makes it possible to group all the tests since these individual tests had different critical discharges. In a similar manner, the distance of the individual marked stones from the toe (L_i) is also normalized with the total chute length (L_s) to represent the displacement in the *x-direction*. dZ which is the displacement in the *z-direction* has also been normalized with the nominal riprap size (d_{50}).

From *Figure 20* which shows the combined buckling-like pattern for all the tests, it is observed how the marked stone at the toe of the riprap (*MS 1750*) undergoes no displacement in the *x-direction*. This is attributed to the fact that the entire riprap was supported at the toe which prevented movement in the *x-direction*. This part represented the pinned end of the column as given in the Euler theory. Moving up the riprap from *MS 1400* through to the top at *MS 0*, it is observed how the 2D displacement of these stones behave which creates the buckling-like pattern as presented in the figure. This figure is a combination of all tests. Individual 2D deformation with buckling-like patterns for each test is presented in the appendix.

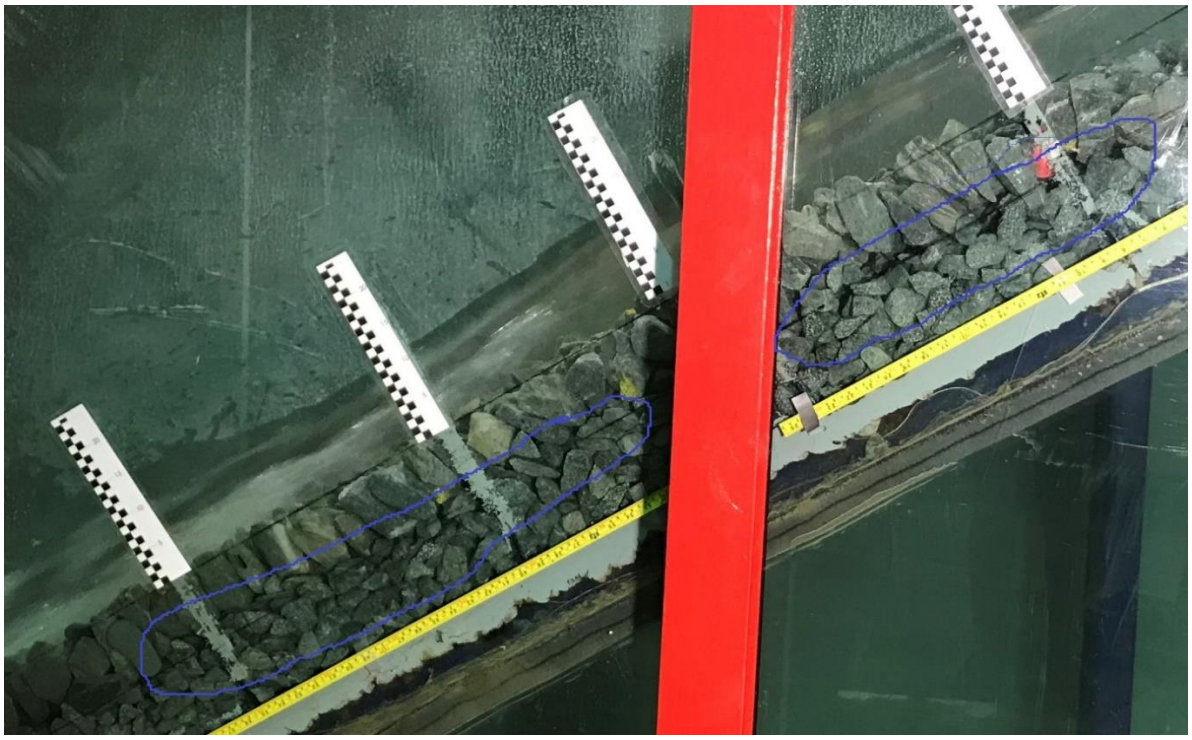

Figure 20 Overtopping test with clear separation between riprap layer and the underlying filter layer which shows how the riprap has unstabilized with the 2D deformation resembling buckling.

During the overtopping tests, it could clearly be seen how the riprap layer had deformed out of the plane of the slope resulting in a buckling-like behavior. This caused a clear separation between the riprap layer and the filter as shown in Figure 21. This tend to affirm the findings which suggest progressive 2D displacement of placed riprap stones as the source of failure in placed riprap.

6.3 Effects of Loading on Riprap Behavior

The applied loads from the water overtopping the riprap in the tests causes some changes to the riprap layer. From the general overtopping loading profile observed at the riprap toe as shown in Figure 16, it is observed that when loading is applied to the riprap layer by overtopping the layer, the initial reaction registered on the load cells, which is just due to the self-weight of the riprap stones moves up to a point and then when the load is removed (pump switched off) the load does not return to the initial value but a value higher than the initial value. As shown in Table 5 which is the broken down reaction pattern observed at the toe for one of the tests, it is seen that prior to overtopping when q_i is 0, the initial total load is 125 N. When the setup is overtopped with a q_i of 50 m^2/s, the load increases to 295 N and when the pump is switched off after the testing time has elapsed, the load reduces until 251 N which has been termed the relief load. This means that for

the incremental discharge of 50 m^2/s, there was a total hydraulic load (*THL*) of 170 *N* which is the difference between the total load and the initial load. The relief load which is the new initial load after the load is removed also means that there has been a compression effect load of 126 *N* which is simply the difference between the relief load and the initial load at $q_i = 0$. The load change which is the difference between the *THL* and the compression effect load is actually the portion of the total hydraulic load which diminishes when the source of load is cut off (pump switched off). This means that overtopping causes a permanent deformation to the structure.

Table 5 Table showing the variation of the different load types with incremental discharge for an overtopping test (Test 2).

q_i (m^2/s)	Total load (N)	Relief Load (N)	THL (N)	Comp. Effect (N)	Load change (N)
0	125				
50	295	251	170	126	44
75	399	324	274	199	75
100	485	372	360	247	113
125	558	450	433	325	108
150	626	477	501	352	149
175	705	567	580	442	138
200	732	554	607	429	178
	755				

This change in the load value is attributed to the fact that at the onset of overtopping, the initial load recorded is valid for dry setup conditions but after overtopping the setup, the riprap stones become wet hence the wetness influencing the initial load value. The wetness of the riprap stone can cause a slight change in the self-weight of the riprap. Also, from the load generation at the riprap toe during building of the riprap, it is realized that there is a certain threshold length ($0.7m$) beyond which any further addition did not cause any significant change in the load registered at the toe of the riprap. As also earlier discussed under failure of the riprap, it has been established that riprap stones underwent a series of displacements during overtopping which causes compaction of stones at the toe of the riprap and a loosening of the stones on the upper part of the chute. This movement of the stones means that some stones move across the threshold line and enters the region where stones actually have impact on the load generated at the riprap toe.

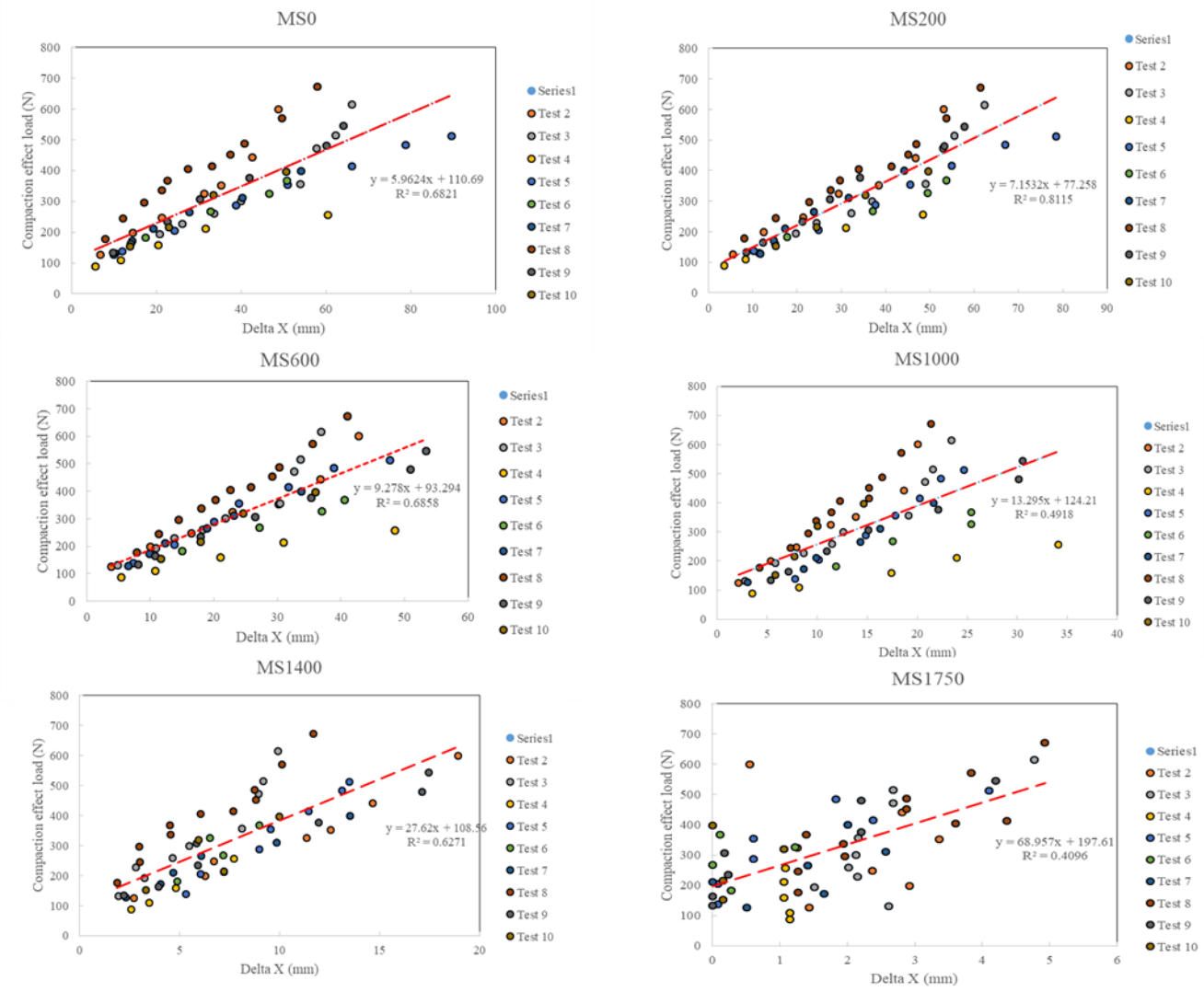

Figure 21 Graphs showing the x-direction displacements of marked stones against the recorded compaction effect load with a linear fit for all tests.

To ascertain that displacement of riprap stones is one of the major cause of permanent deformation in riprap loading, displacement of marked riprap stones have been compared with the compaction effect loads recorded for all the tests. It is observed that the compaction effect load increases with an increase in the displacement of the marked stones. All marked stones showed a good cluster of the values with a clear trend which shows how the compaction effect load is proportional to the displacement in the *x-direction* for all the tests as shown in Figure 22 except for marked stone *MS*1750 which is the last stone at the toe. This shows a relation which is not linear because the entire riprap is supported at the toe and this support restricts displacement of the stones in that

area. It is also observed that delta *x* values for the marked stones increases with the position of the stone with stones farthest from the supported toe recording maximum *x* displacements and vice versa.

The individual marked stone displacements were also analyzed with regards to the incremental discharges for each test. Similar to the compaction effect load, higher incremental discharges resulted in higher stone displacements with stones closer to the supported toe experiencing little to no displacement while those farthest away from the toe underwent high displacements and also displacements increased as discharge increased. From *Figure 23*, it is seen how displacement increased with increasing discharge. It is also seen that individual marked stones behaved differently when subjected to the discharges. This is because local situations affected the movement of these stones. As seen from the graph, *MS1750* which is located just at the toe of the riprap where the entire riprap is supported underwent just minor movements. Sometimes these movements were even oscillatory where there was a back and forth movement of that marked stone. Individual graphs for all the tests are shown in the appendix.

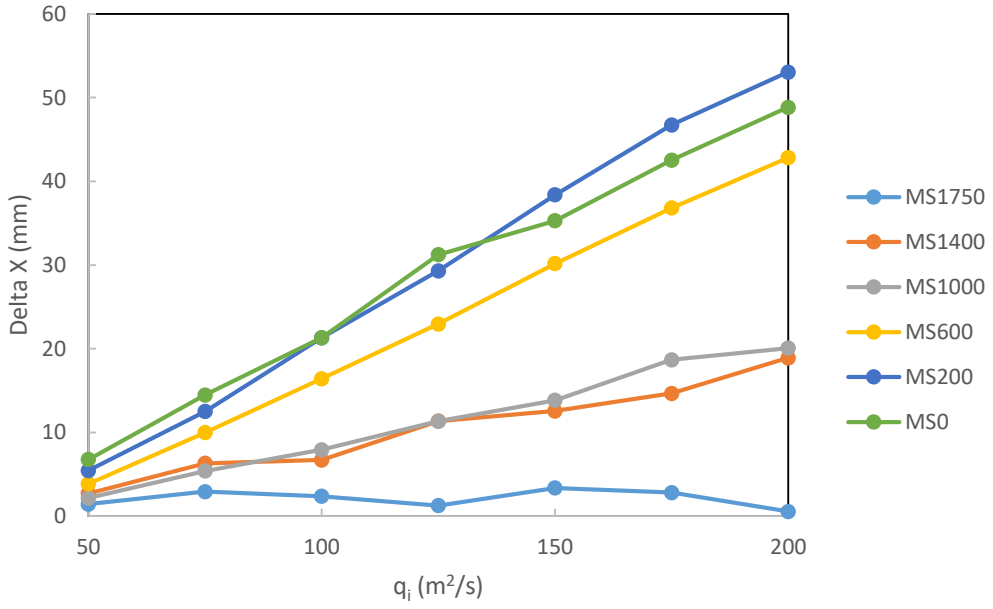

Figure 22 Difference in the displacement of the different marked stones with incremental discharge.

With regards to the loading recorded at the toe of the riprap, it is seen that the three different loads discussed earlier behaves differently with increasing discharge. In this section, all the different

loads recorded from the tests have been put together to check how these loads change with increasing discharge. Detailed load trends for all tests are given in the appendix. From Figures 24, 25 and 26 it is realized that the total hydraulic and compaction effect loads both increases as the discharge is increased. The third load condition which is the change in load increases with increasing discharge to a point and then stabilizes.

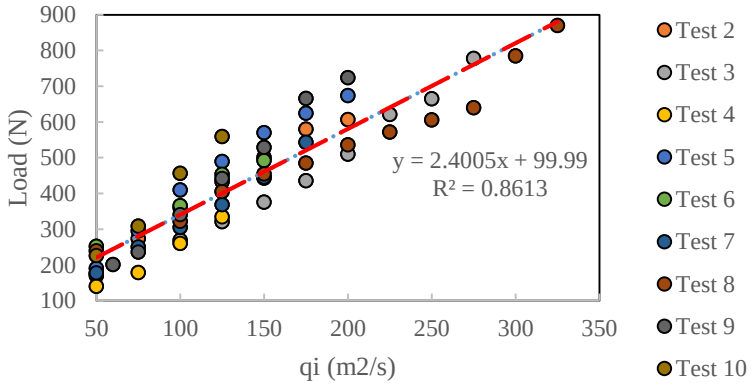

Figure 23 Trend of the Total Hydraulic Load for all tests as observed showing clear increase of the load with increase in discharge.

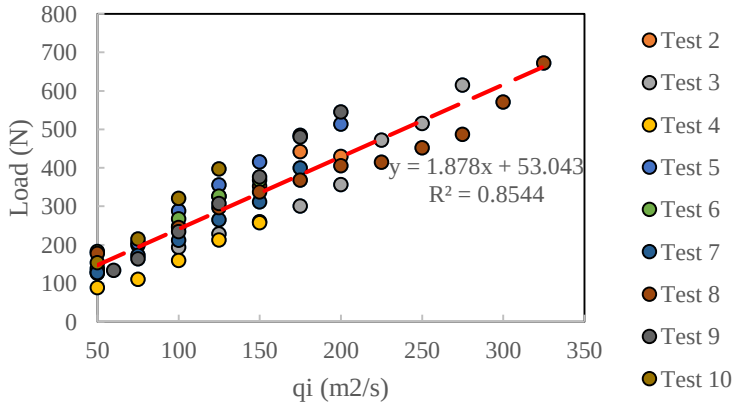

Figure 24 Trend of the Compression Effect Load for all tests as observed showing increase in the compression effect on the riprap with increase in discharge.

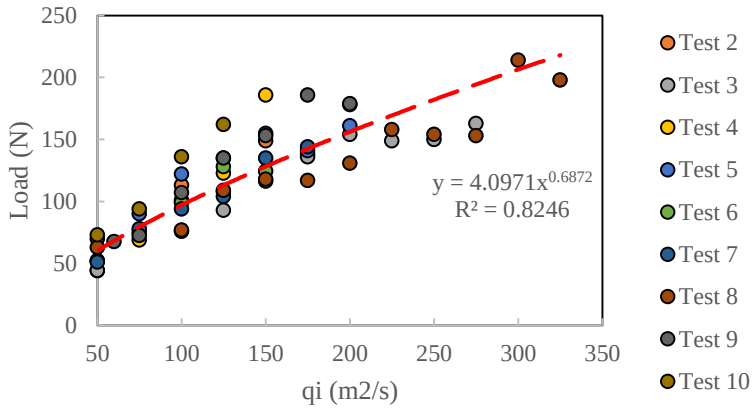

Figure 25 Trend in the Change in Load which is the difference of the THL and the compression effect load for all tests where it is seen that for higher discharges, there is stabilization of the load.

Loads measured at the toe section of the embankment have been groups into three. The Total Hydraulic Load, the Compression Effect Load and the difference of this two which is the change in load as defined earlier in this chapter. These three loads behaved differently with discharge with the THL and the compression effect loads increasing with increasing discharges as depicted in Figures 24 and 25 whereas on the other hand their difference which is the change in load increases with increase discharge to a point and then stabilizes at high discharges as seen in Figure 26.

7.0 CONCLUDING SUMMARY AND RECOMMENDATIONS

This study has increased knowledge of load generation mechanism and general failure mechanism at the toe section of placed riprap on steep slopes exposed to overtopping flow. Placed riprap where stones are placed one by one in an interlocking pattern is not very common all over the world but the technology is gradually gaining prominence in some developed countries like Norway. There has been extensive research into dumped riprap and also riprap on gentle slopes. Research on placed riprap and ripraps on steep slopes ($S > 50\%$) are scarce and so are those focused on the toe section of the entire riprap structure as revealed in the literature review. The entire study has addressed the objectives of this thesis outlined in *Section 1.2*.

Physical model investigations were planned on the existing physical model in the hydraulics laboratory in the department to study the dynamic loading mechanism at riprap toe section. This was achieved by the installation of a load cell at the base of the riprap layer to monitor the load generation and variation with time and also with incremental discharges during the overtopping tests. Measured riprap parameters compared to values from Hiller et al. (2017) showed slight alterations in these parameters due to wearing of the stones as it has been used for a number of tests. Load generated at the riprap toe was seen to be as a result of the riprap stone self-weight (geotechnical) and the water that overtops the setup (hydraulic). It is observed that during building of the riprap structure, the weight of the individual stones have an effect at the toe of the structure as the riprap is built from the toe upwards. Beyond a threshold distance of 0.7 meters from the toe, any additional stone placed has no significant effect at the toe. This means that during building of the riprap the load recordings at the toe tend to stabilize at a specific distance from the toe which in this case is 0.7 meters from the base. It is also established that the underlying filter layer of the riprap, the walls of the flume and the interlocking forces that exists between the placed riprap stones offers a great deal of resistance to the weight of the stones acting at the toe of the riprap. The geotechnical load at the toe of the riprap is present at the onset of overtopping of the dam crest. The nature and magnitude of this initial load is altered after the riprap is further compacted after being exposed to overtopping.

A number of overtopping tests carried out showed that overtopping causes two dimensional displacements of riprap stones. This two dimensional displacement causes the riprap stones (which due to the interlocking forces between them are acting as one bearing structure) to progressively

deform in a buckling-like pattern which eventually leads to the total collapse of the entire riprap. The x-displacement or displacements along the length of the slope causes compaction of the riprap stones at the toe since the entire riprap structure is supported at the base. This compaction of the riprap stones cause the initial geotechnical load present at the toe of the riprap at the onset of overtopping to increase and does not return to its initial value even if the source of loading which is overtopping is stopped. Overtopping in general causes a total hydraulic load to act the riprap toe as recorded from the load cells. This total hydraulic load has a compaction effect that causes the initial geotechnical load to increase even if the source is cut off. For incremental discharges, the total hydraulic load and its compaction effect all increase as the discharge is also increased. The excess of the total hydraulic load which is the difference of the total hydraulic load and the compaction effect load also increases with the two loads from lower discharges then tend to stabilize for higher discharges.

It is worthy of note that this finding is valid for placed riprap on steep slope ($S = 0.67$) supported at the toe. This finding has helped established some load generation mechanisms for the conditions specified above. For a generalized and sound conclusion to be made for placed ripraps, it is recommended that further studies be carried out on milder slopes and unsupported toes so to compare results and make general conclusions. Overtopping of the riprap was also done in a gradual increasing manner the outflow hydrograph of which may not resemble the outflow hydrograph of a dam experiencing extreme loading conditions caused by flooding or landslide induced tsunamis in the reservoirs that these dams create. Therefore it is further recommended that more tests be carried out with different outflow hydrographs to check the behavior of the riprap is all these scenarios to help understand this subject matter into detail.

REFERENCES

Norwegian Water and Energy Directorate (NVE), N.W.R. and E.D., 2012. Guideline for embankment dams.

Abt, S.R., Johnson, T.L., Thornton, C.I., Trabant, S.C., 1998. Riprap Sizing at Toe of Embankment Slopes. J. Hydraul. Eng. 124, 672–677. https://doi.org/10.1061/(ASCE)0733-9429(1998)124:7(672)

Abt, S.R., Thornton, C.I., Gallegos, H.A., Ullmann, C.M., 2008. Round-shaped riprap stabilization in overtopping flow. J. Hydraul. Eng. 134(8).

Bunte, K., Abt, S.R., 2001. Sampling Surface and Subsurface Particle-Size Distributions in Wadable Gravel- and Cobble-Bed Streams for Analyses in Sediment Transport , Hydraulics , and Streambed Monitoring. 0 450. https://doi.org/10.1017/CBO9781107415324.004

Dornack, S., 2001. Overtoppable dams - design criteria for riprap/ (PhD Thesis, T.U. Dresden).

Hiller, P.H., Aberle, J., Lia, L., 2017. Displacements as failure origin of placed riprap on steep slopes. J. Hydraul. Res. 1686, 1–15. https://doi.org/10.1080/00221686.2017.1323806

ICOLD, 1995. Dam failures statistical analysis. International Commission on Large Dams (ICOLD) bulletin no. 99.

Khan, D., Ahmad, Z., 2011. Stabilization of Angular-Shaped Riprap under Overtopping Flows. World Acad. Sci. Eng. Technol. Int. J. Civil, Environ. Struct. Constr. Archit. Enfineering 5, 550–554.

Linford, A., Saunders, D.H., 1967. A hydraulic investigation of through and overflow rockfill dams (Report No. RR888). British Hydromechanics Research Association.

Moran, Rafael.; Toledo, M.A., 2011. Research into protection of rockfill dams from overtopping using rockfill downstream toes. Can. J. Civ. Eng.

Moran, R., 2015. Review of embankment dam protections and design methodology for downstream rockfill toes. pp. 25–39.

Pfister, M., Chanson, H., 2012. Scale effects in physical hydraulic engineering models by Valentin Heller. J. Hydraul. Res. 49.

Ravindra, G., Sigtryggsdottir, F., Lia, L., 2018a. Buckling of placed ripraps on steep slopes exposed to overtopping. J. Hydraul. Res.

Ravindra, G., Sigtryggsdottir, F., Lia, L., 2018b. Evaluation of design criteria for downstream riprap of rockfill dams., in: Twenty Fifth Congress of ICOLD. Vienna.

Ravindra, G.H.R., Sigtryggsdottir, F.G., Lia, L., 2018. Protection of embankment dam toe and abutments under overtopping conditions 6–8.

Siebel, R., 2007. Experimental investigations on the stability of riprap layers on overtoppable earthdams. Environ. Fluid Mech. 7, 455–467. https://doi.org/10.1007/s10652-007-9041-8

Solvik, O., 1991. Throughflow and stability problems in rockfill dams exposed to exceptional loads., in: Sixteenth International Congress on Large Dams. pp. 333–343.

Sommer, P., 1997. Overtoppable erosion protections. Unpublished report No. DFG-Forschungsbericht La 529/8-1, Universitat Karlsruhe.

Thornton, C.I., Abt, S.R., Scholl, B.N., Bender, T.R., 2014. Enhanced Stone Sizing for Overtopping Flow. J. Hydraul. Eng. 140, 1–4.

Toledo, M.A., Moran, R., Onate, E., 2015. Dam protections against overtopping and accidental leakage. London: CRC Press / Balkema.

Williamson, T., 2017. Historic dam failures and recent incidents. Eng. Irel.

APPENDICES

APPENDIX 1: TEST 2

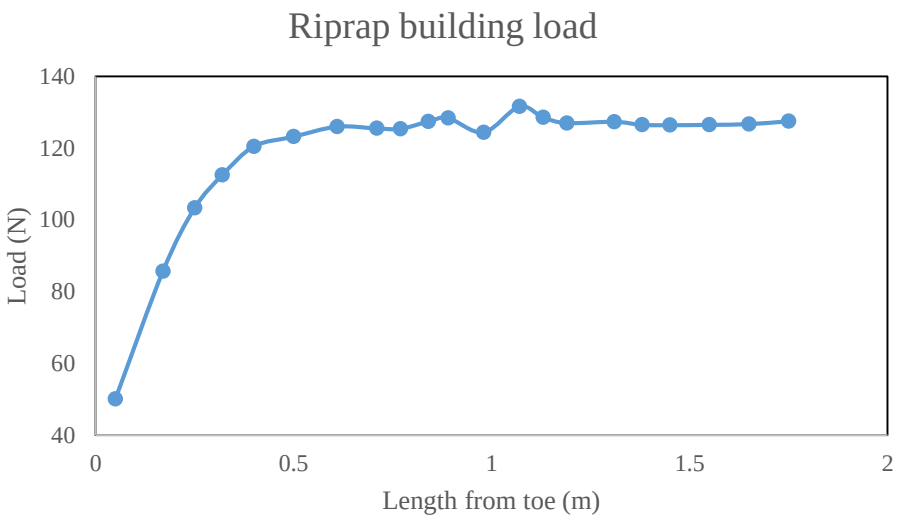

Effect of riprap stone self-weight felt at the toe of the riprap during riprap construction.

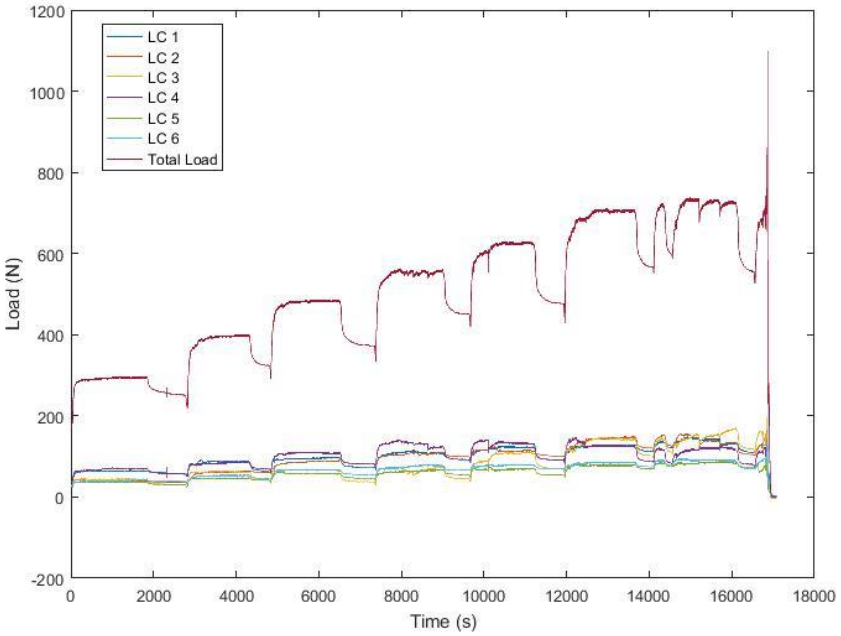

Load profile for test 2 as recorded by the load cells after the overtopping test

Table showing loading values for all incremental discharges during overtopping test for test 2.

q_i (m^2/s)	Total load (N)	Relief Load (N)	THL (N)	Comp. Effect (N)	Load change (N)
0	125				
50	295	251	170	126	44
75	399	324	274	199	75
100	485	372	360	247	113
125	558	450	433	325	108
150	626	477	501	352	149
175	705	567	580	442	138
200	732	554	607	429	178
	755				

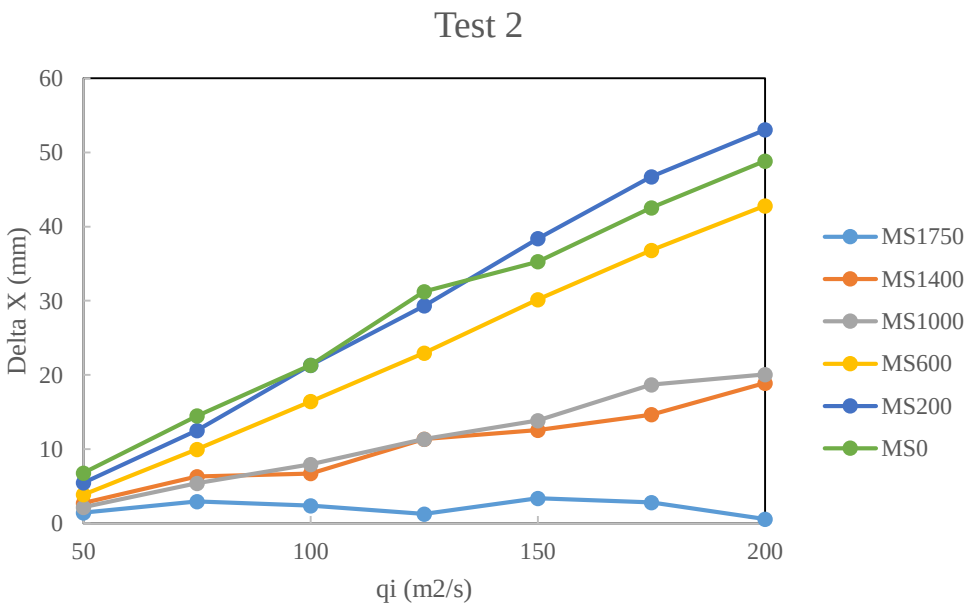

Graph of x-direction displacements with increase in discharge

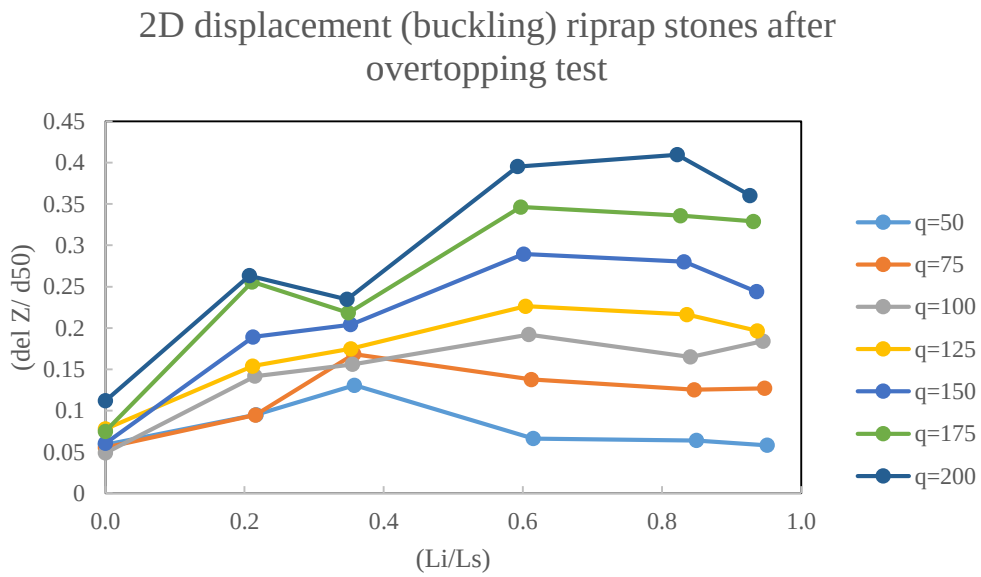

Observed buckling pattern for marked riprap stones

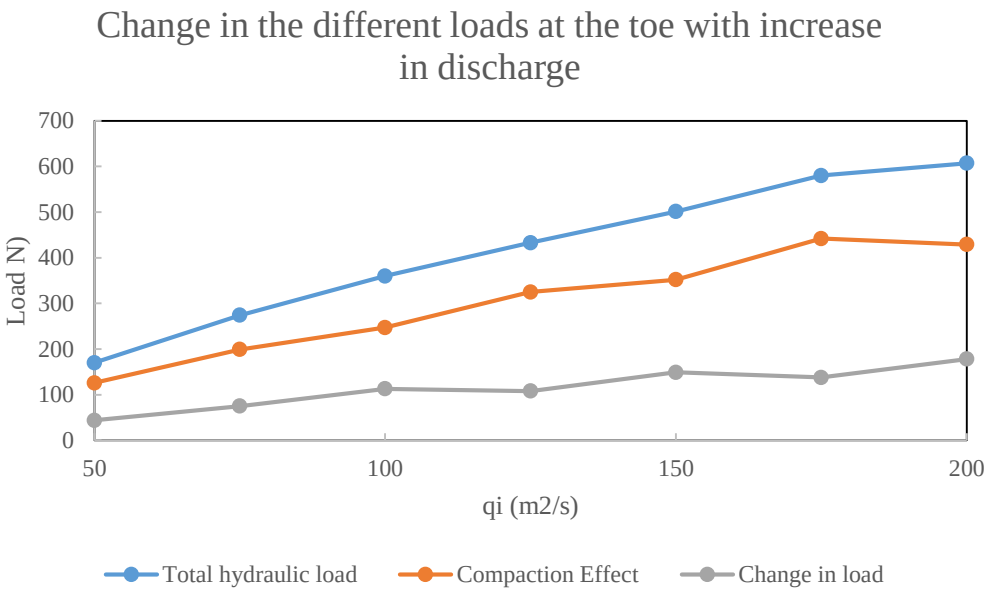

Changes in the different load types with change in the incremental discharges

APPENDIX 2: TEST 3

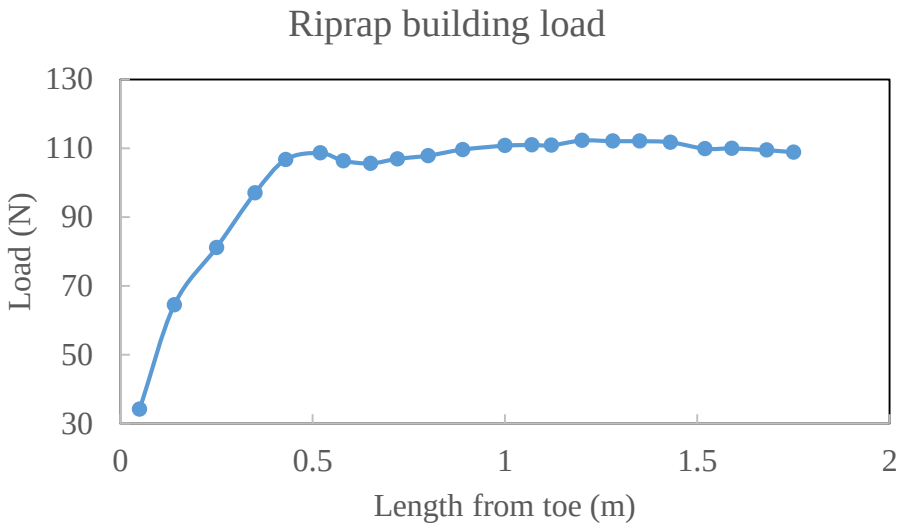

Effect of riprap stone self-weight at the toe of the riprap during riprap construction.

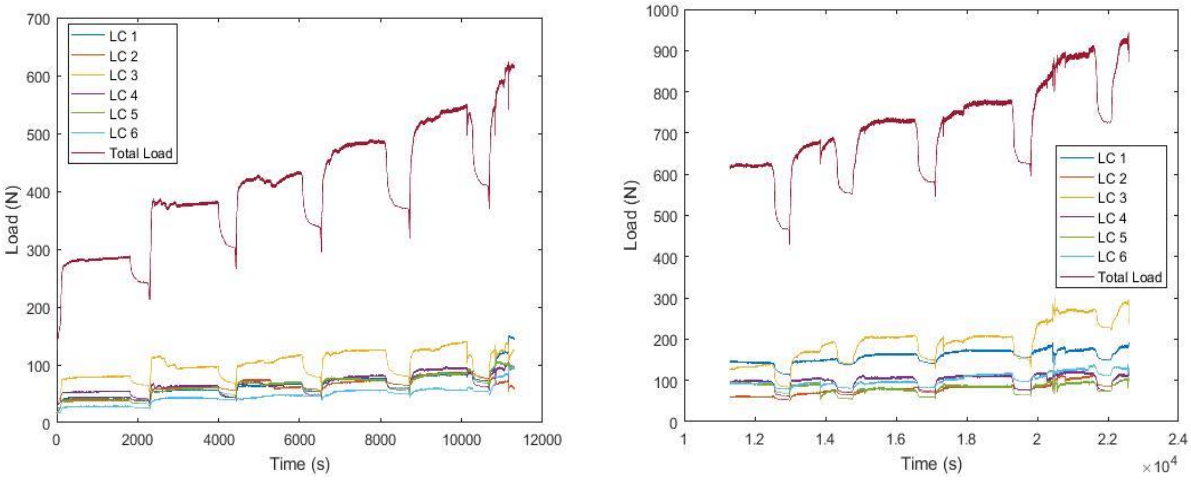

Load profile for test 3 as recorded by the load cells after the overtopping test.

Table showing loading values for all incremental discharges during overtopping test for test 3.

q_i (m^2/s)	Total load (N)	Relief Load (N)	THL (N)	Comp. Effect (N)	Load change (N)
0	110				
50	285.5	241	175.5	131	44.5
100	379	303	269	193	76
125	431	338	321	228	93
150	486	369.5	376	259.5	116.5
175	546	410	436	300	136
200	620	466	510	356	154
225	731	582	621	472	149
250	775	625	665	515	150
275	888	725	778	615	163
	924				

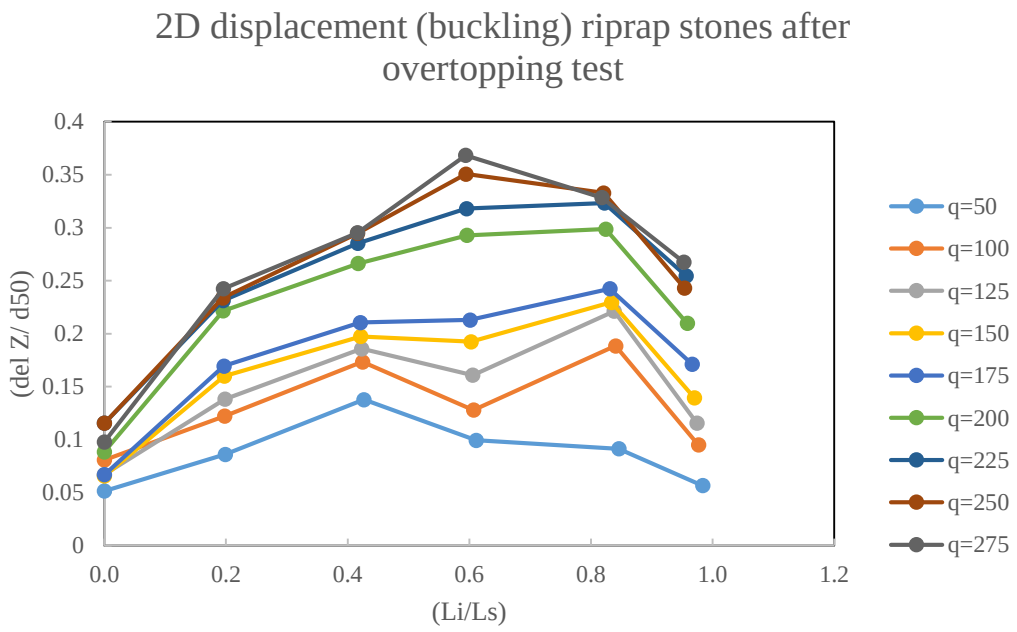

Observed buckling pattern for marked stones for test 3.

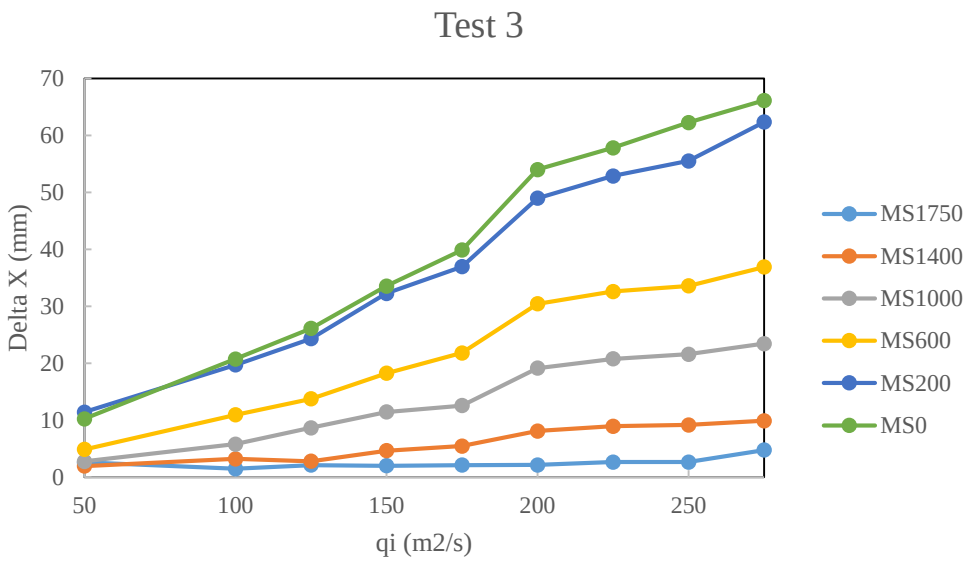

Graph of x-direction displacement with increase in discharge for the marked stones.

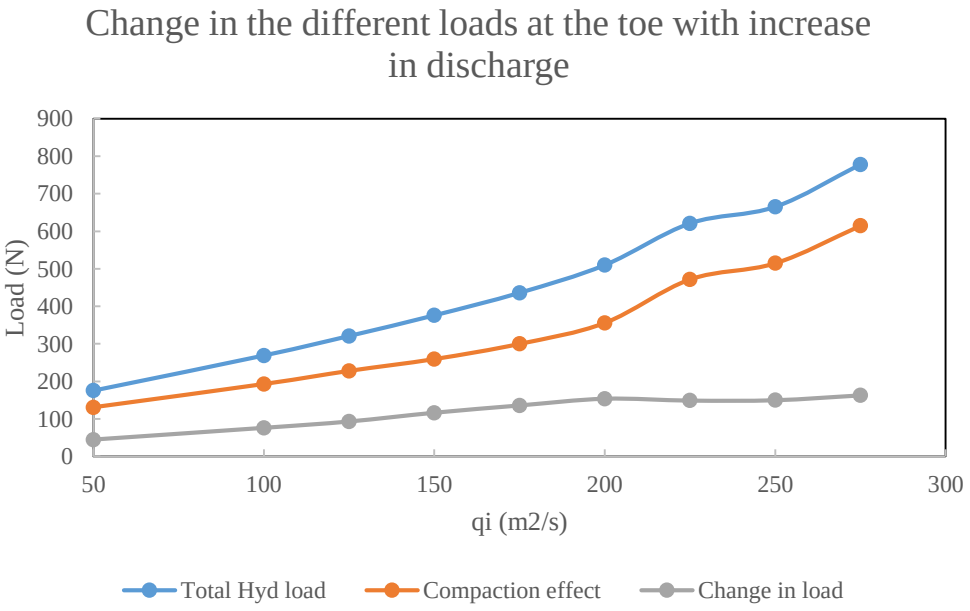

Change in the different loads with increasing incremental discharge for test 3.

APPENDIX 3: TEST 4

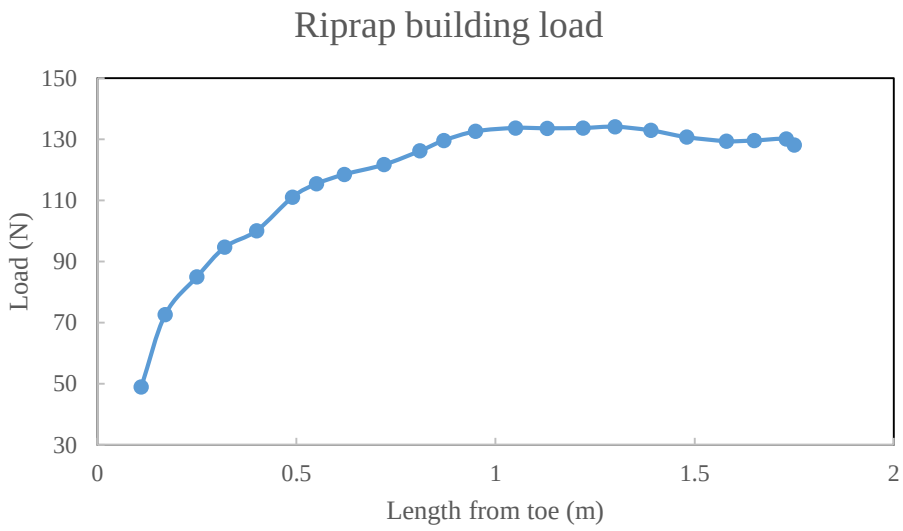

Effect of riprap self-weight at the toe of the riprap during riprap construction.

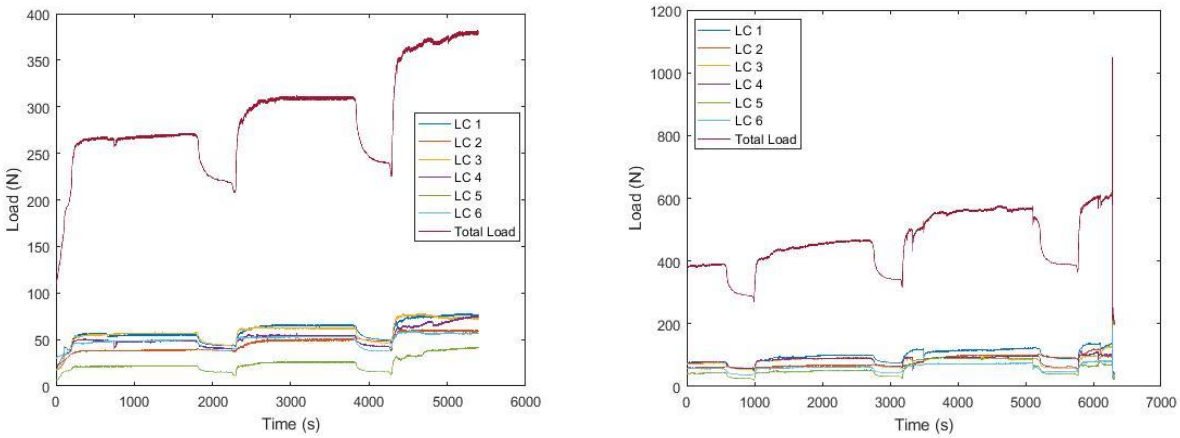

Load profile for test 4 as recorded by the load cells during overtopping test.

Table showing loading values for all incremental discharges during overtopping test for test 4.

q_i (m^2/s)	Total load (N)	Relief Load (N)	THL (N)	Comp. Effect (N)	Load change (N)
0	130				
50	270	218	140	88	52
75	309	240	179	110	69
100	390	289	260	159	101
125	465	342	335	212	123
150	573	387	443	257	186
	621		491		

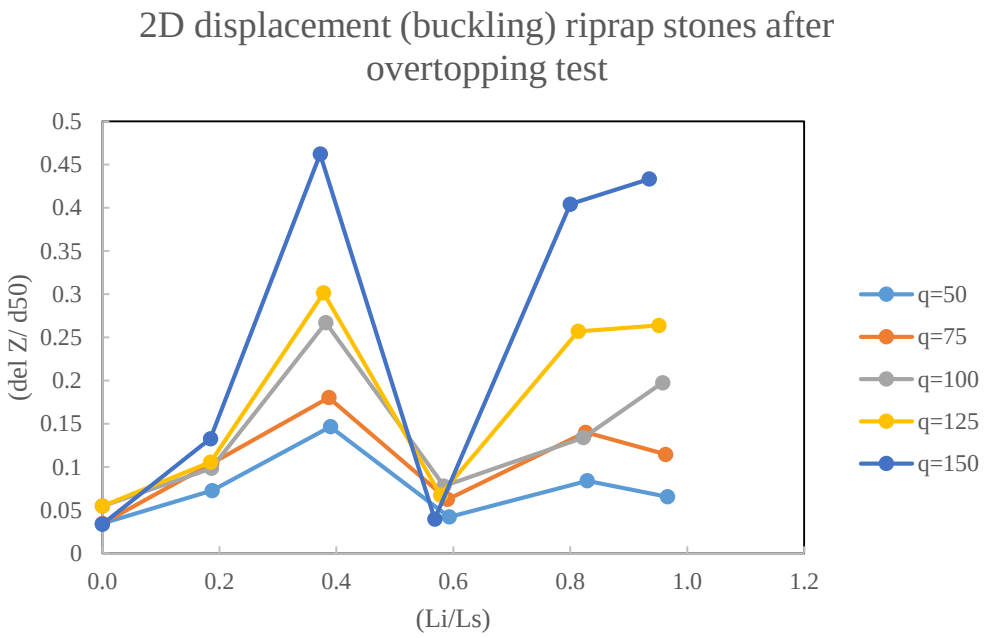

Buckling pattern of marked stones during overtopping for test 4

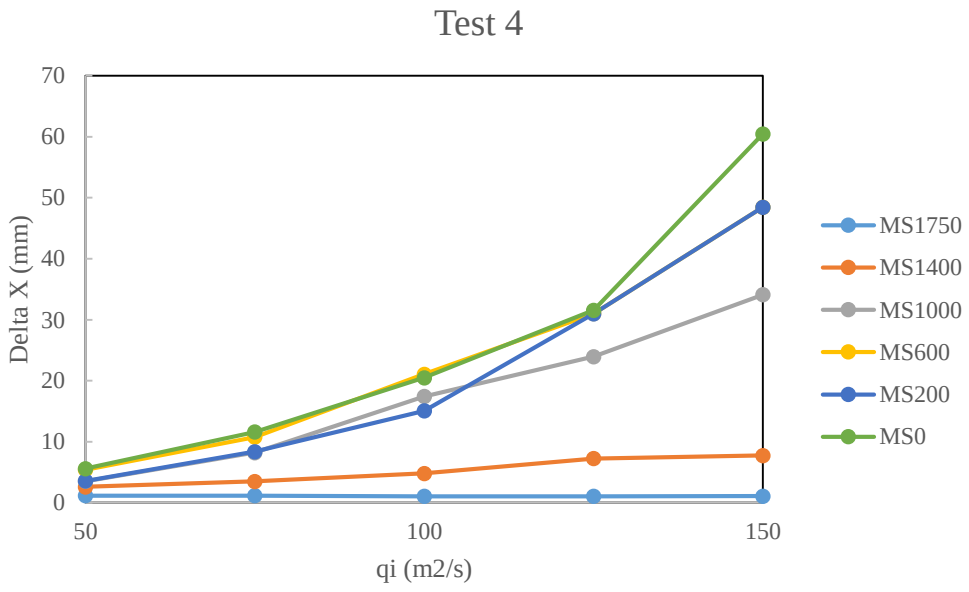

Graph of x-direction displacements with increase in discharge for test 4.

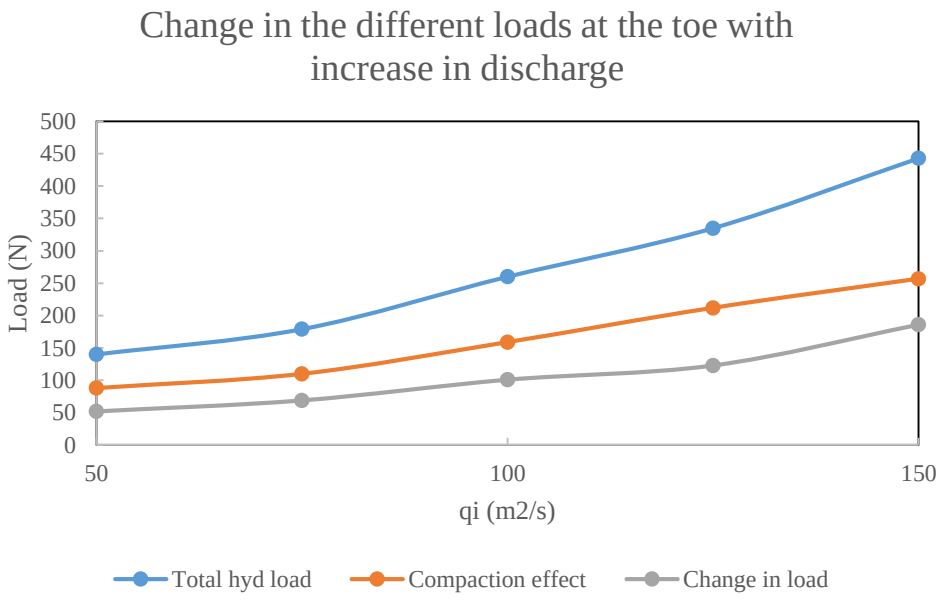

The change in the different loads with change in the incremental discharge for test 4.

APPENDIX 4: TEST 5

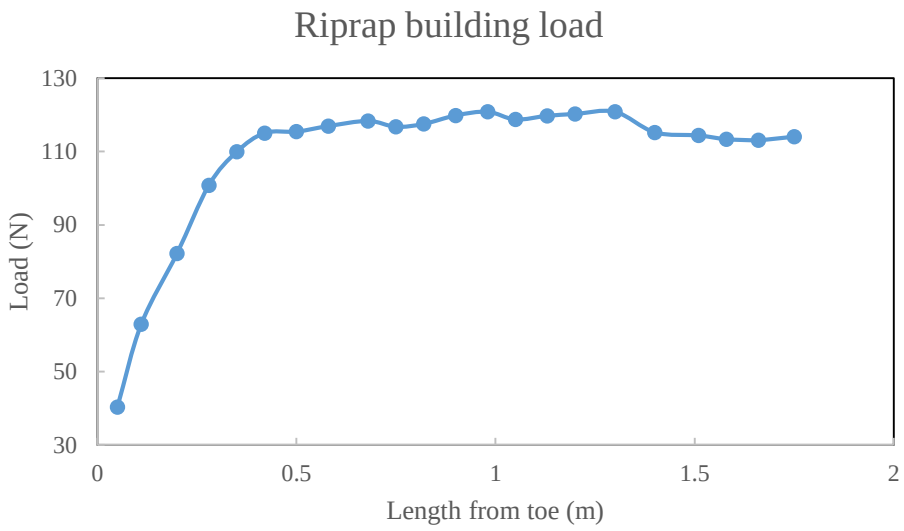

Effect of riprap stone self-weight at the toe of the riprap during riprap construction.

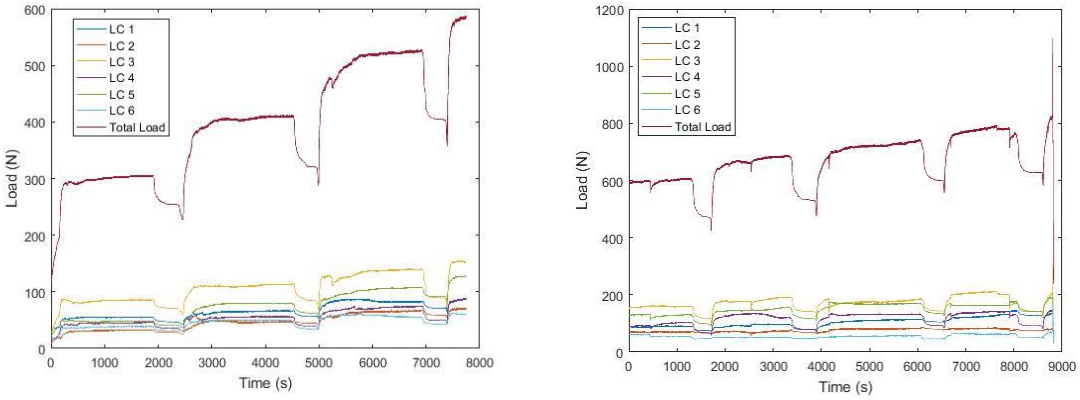

Load profile for test 5 as recorded by the load cells during overtopping test.

Table showing loading values for all incremental discharges during overtopping test for test 5.

q_i (m^2/s)	Total load (N)	Relief Load (N)	THL (N)	Comp. Effect (N)	Load change (N)
0	115				
50	305	253	190	138	52
75	410	320	295	205	90
100	525	403	410	288	122
125	605	470	490	355	135
150	685	530	570	415	155
175	740	599	625	484	141
200	789	628	674	513	161
	818				

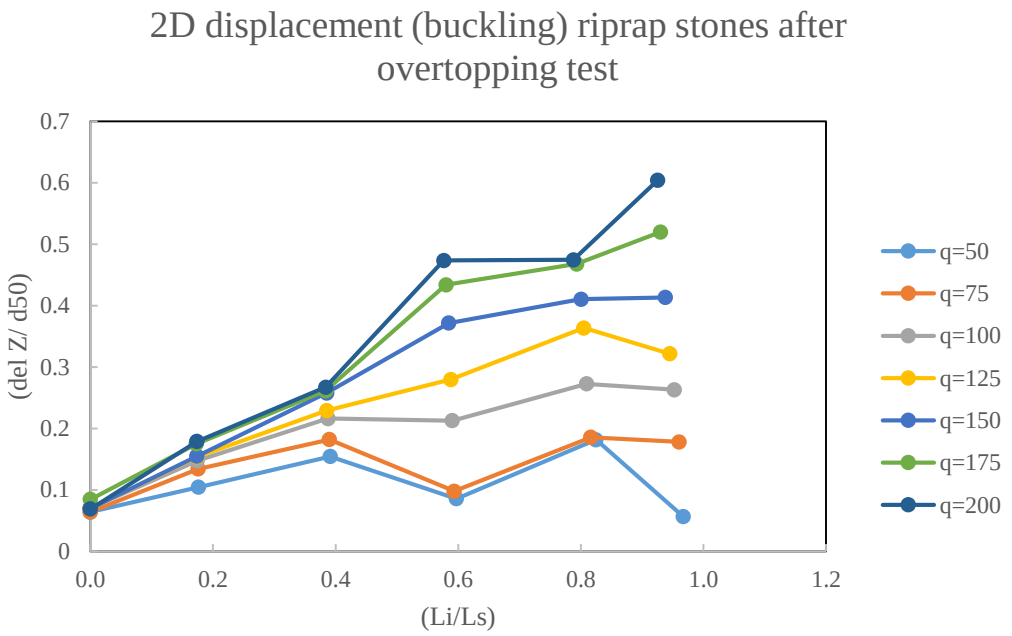

Buckling pattern for marked riprap stones during overtopping test for test 5.

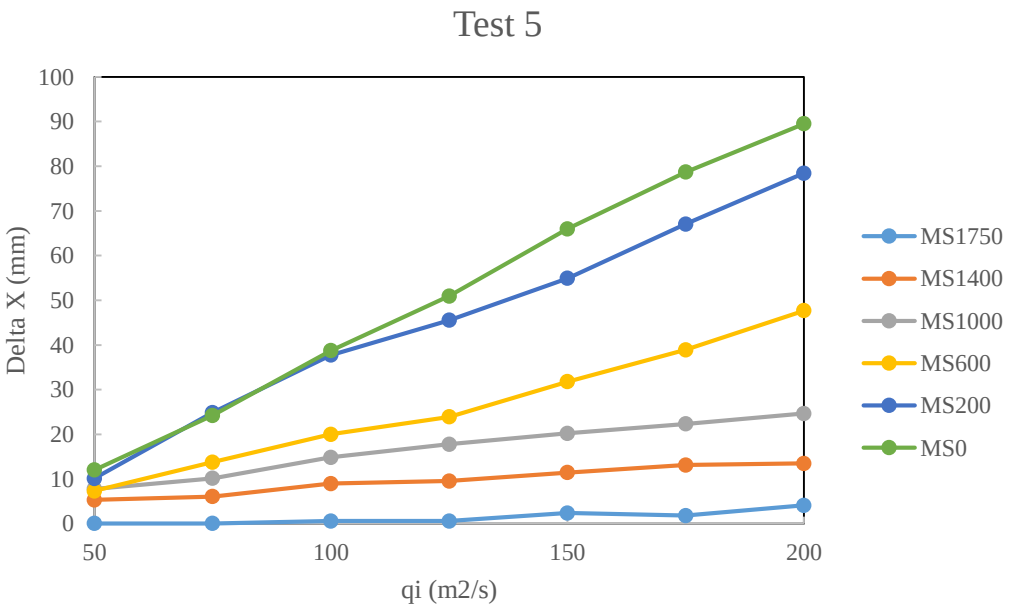

Graph of x-direction displacements with increase in discharge.

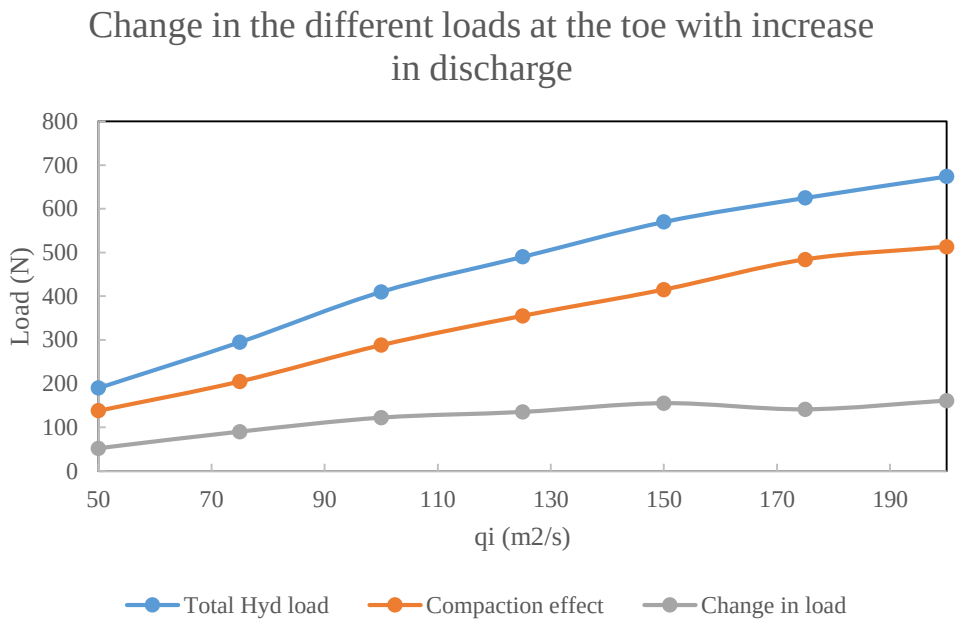

The change in the different loads with change in the incremental unit discharge for test 5.

APPENDIX 5: TEST 6

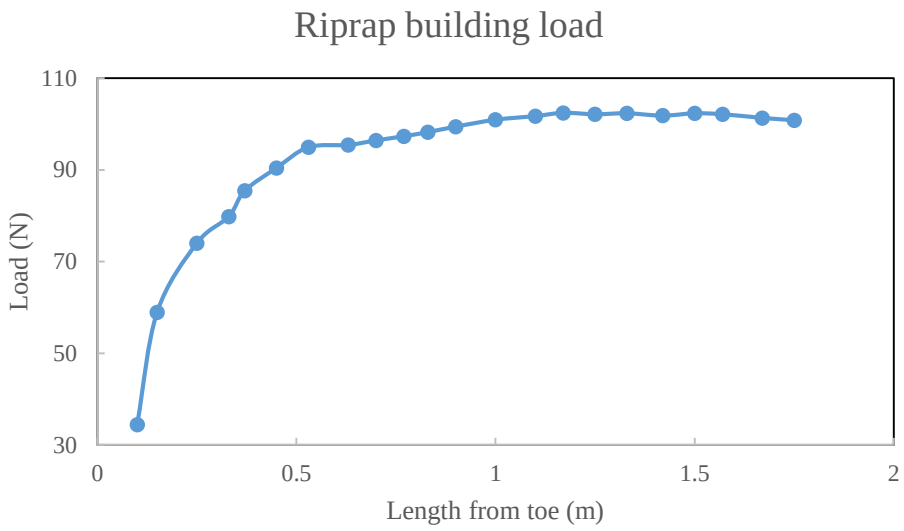

Effect of riprap stone self-weight at the toe of the riprap during riprap construction.

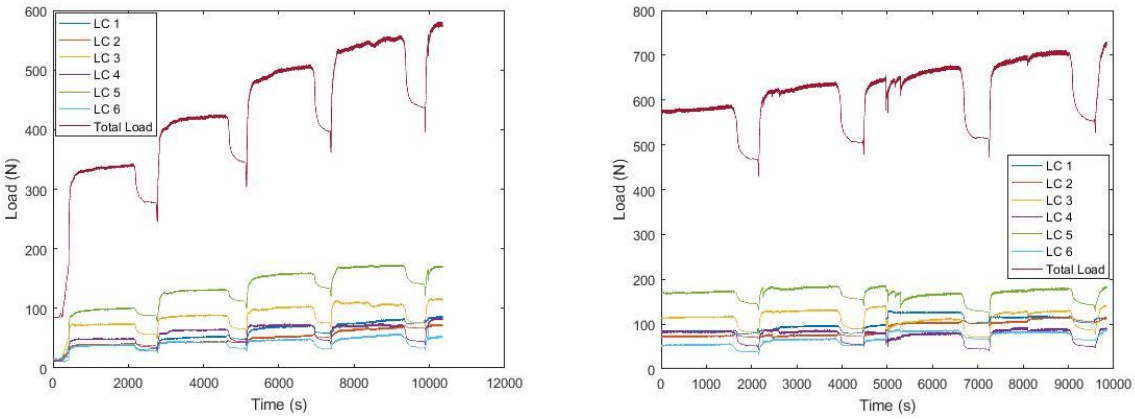

Load profile for test 6 as recorded by the load cells during overtopping test.

Table showing loading values for all incremental discharges during overtopping test for test 6.

q_i (m^2/s)	Total load (N)	Relief Load (N)	THL (N)	Comp. Effect (N)	Load change (N)
0	100				
50	352	282	252	182	70
100	466	367	366	267	99
125	554	426	454	326	128
150	592	467.5	492	367.5	124.5
	655				

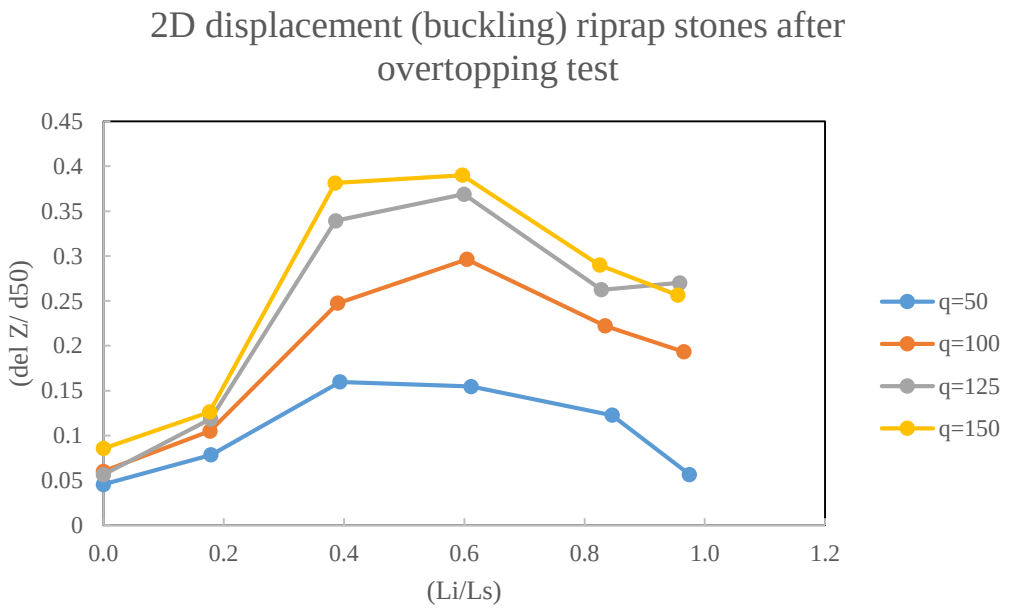

Buckling pattern of marked riprap stones during overtopping test for test 6.

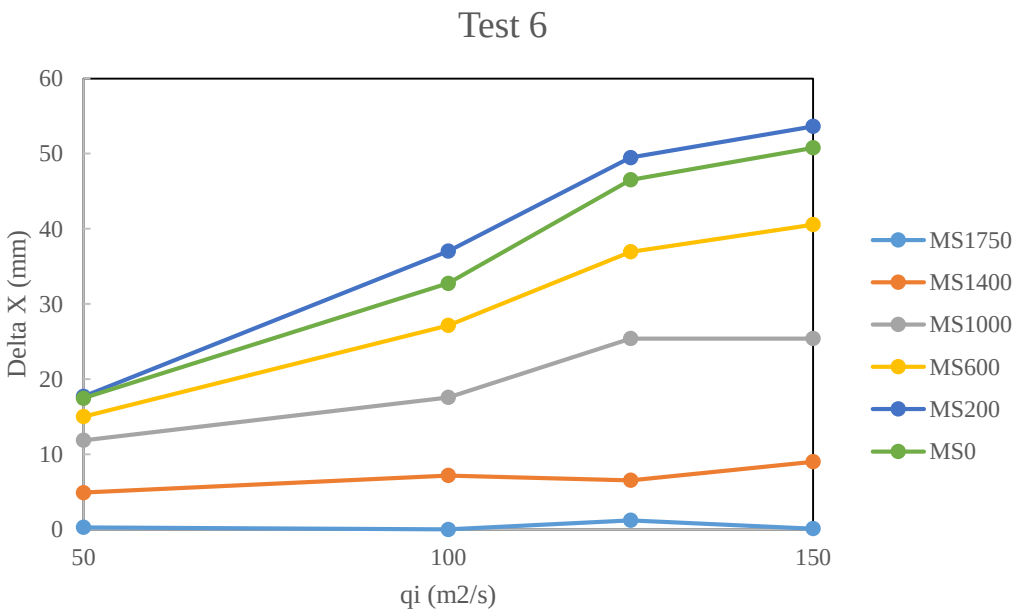

Graph of x-direction displacements with increase in discharge.

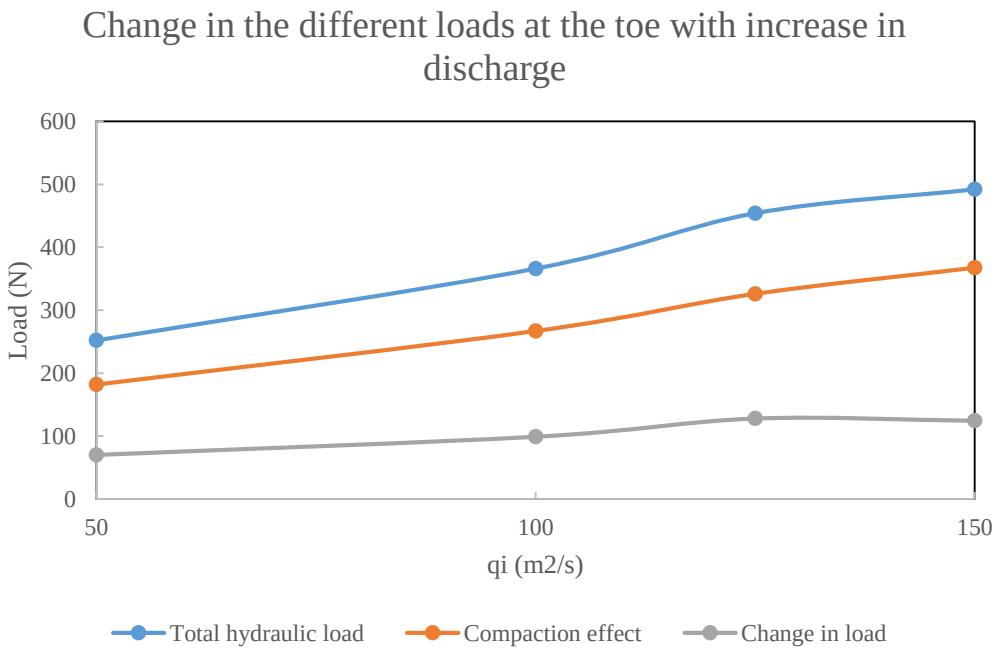

Change in the different loads with change in discharge for test 6.

APPENDIX 6: TEST 7

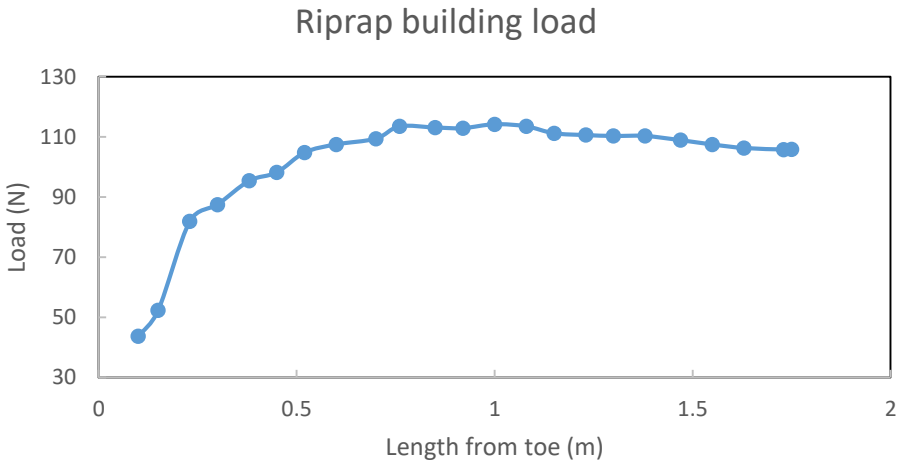

Effect of riprap stone self-weight at the toe of the riprap during riprap construction.

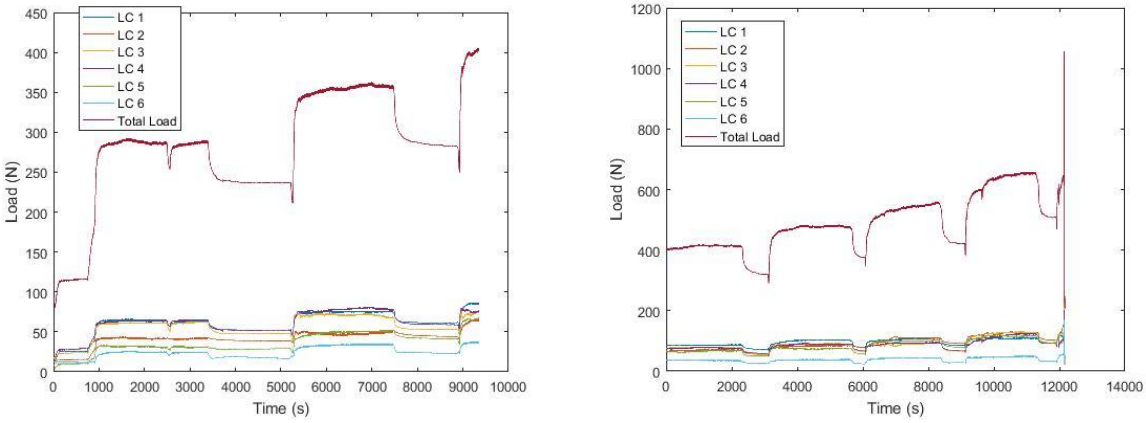

Load profile for test 7 as recorded by the load cells during overtopping test.

Table showing loading values for all incremental discharges during overtopping test for test 7.

q_i (m^2/s)	Total load (N)	Relief Load (N)	THL (N)	Comp. Effect (N)	Load change (N)
0	110				
50	288	237	178	127	51
75	360	282	250	172	78
100	415	321	305	211	94
125	479	375	369	265	104
150	556	421	446	311	135
175	653	509	543	399	144
	645				

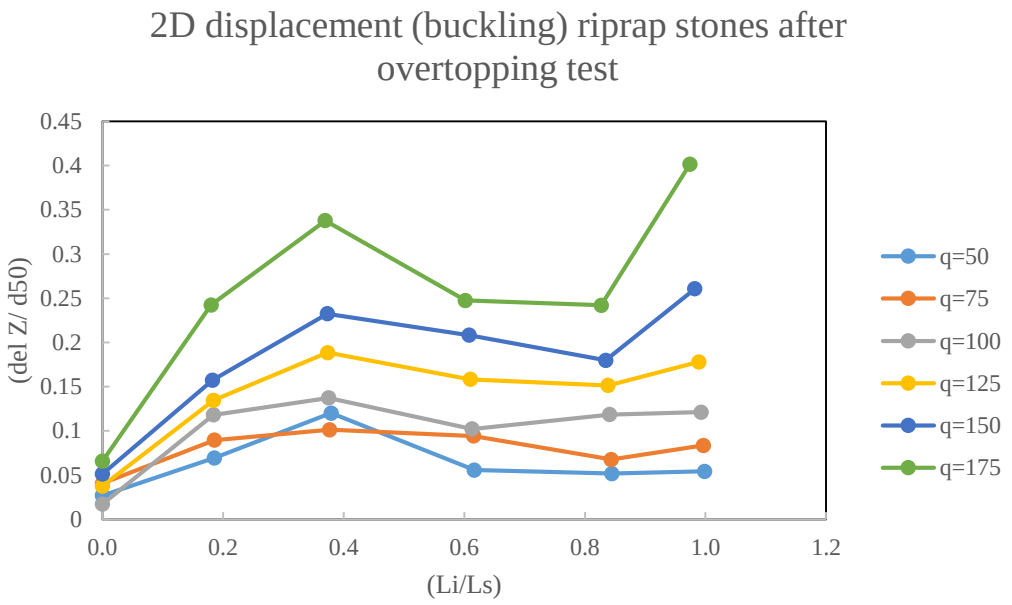

Buckling pattern for marked riprap stones during overtopping test.

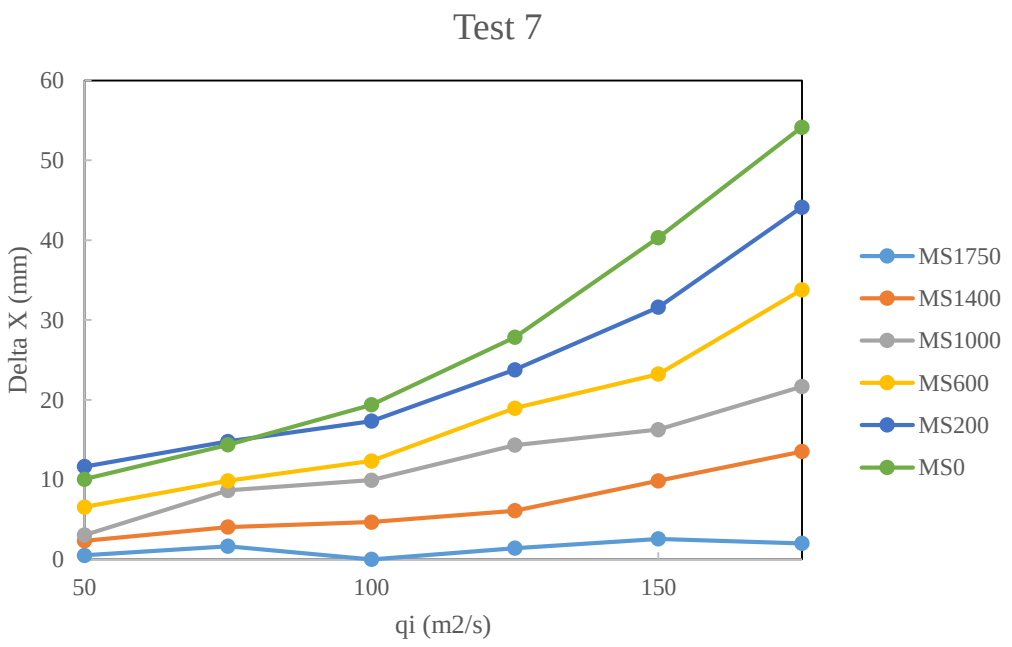

Graph of x-direction displacements with increase in discharge.

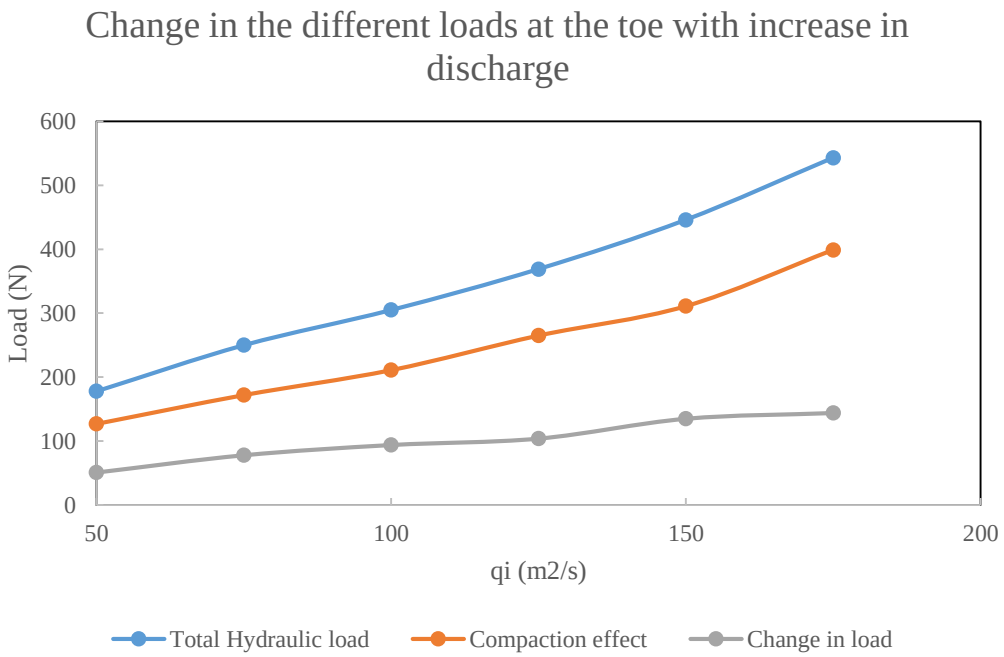

Change in the different loads with change in incremental discharge for test 7.

APPENDIX 7: TEST 8

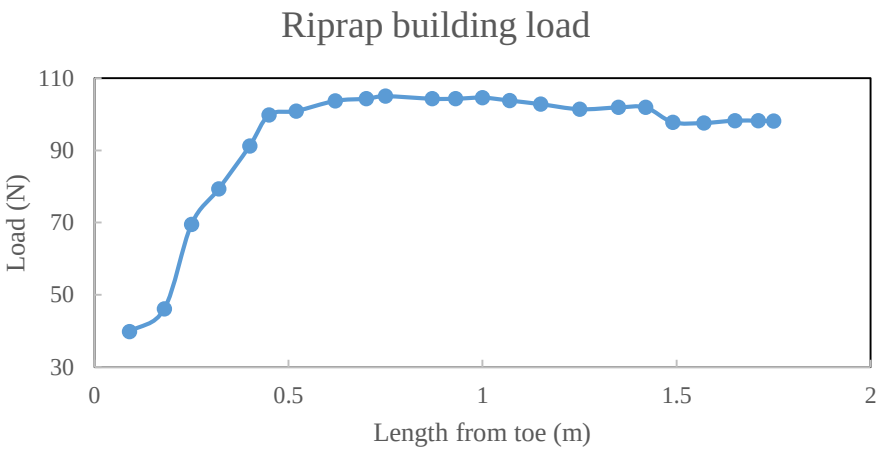

Effect of riprap stone self-weight at the toe of the riprap during riprap construction.

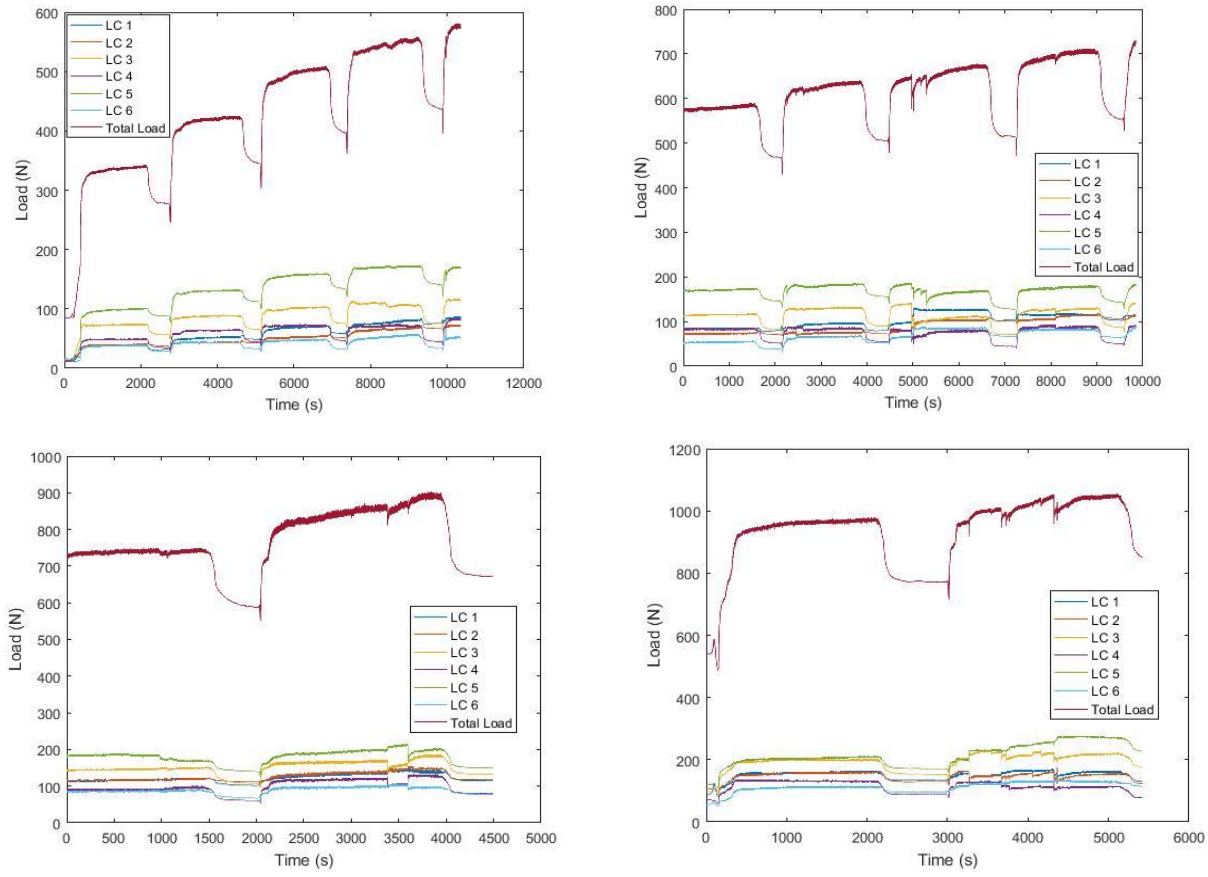

Load profile for test 8 as recorded by the load cells during overtopping test.

Table showing loading values for all incremental discharges during overtopping test for test 8.

q_i (m^2/s)	Total load (N)	Relief Load (N)	THL (N)	Comp. Effect (N)	Load change (N)
0	100				
50	340	277	240	177	63
100	422	345	322	245	77
125	505	396	405	296	109
150	555	437	455	337	118
175	585	468	485	368	117
200	636	505	536	405	131
225	672	514	572	414	158
250	706	552	606	452	154
275	740	587	640	487	153
300	885	671	785	571	214
325	970	772	870	672	198
	1040				

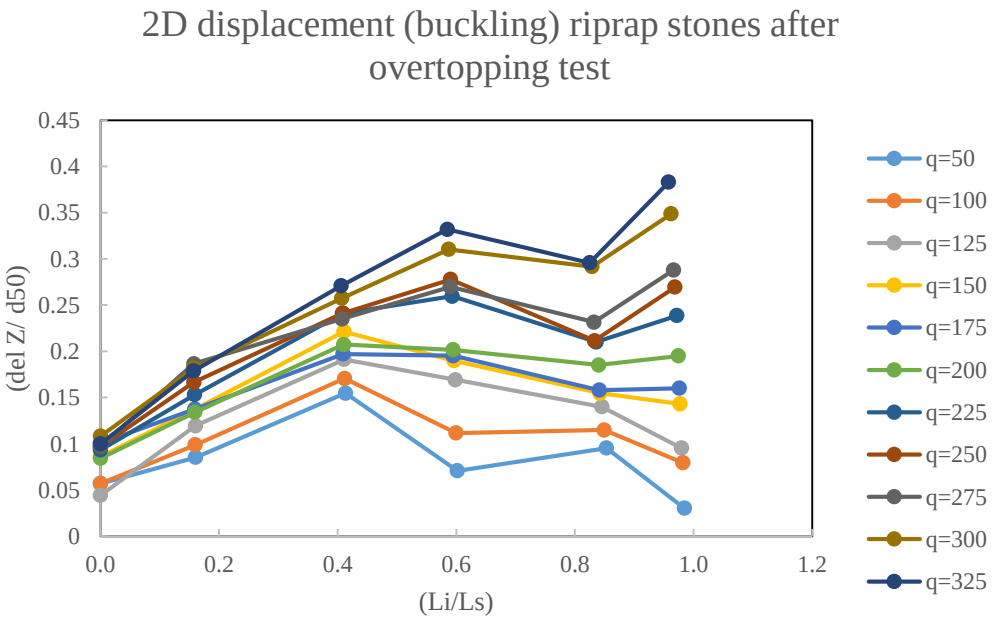

Buckling pattern of marked riprap stones during overtopping test for test 8.

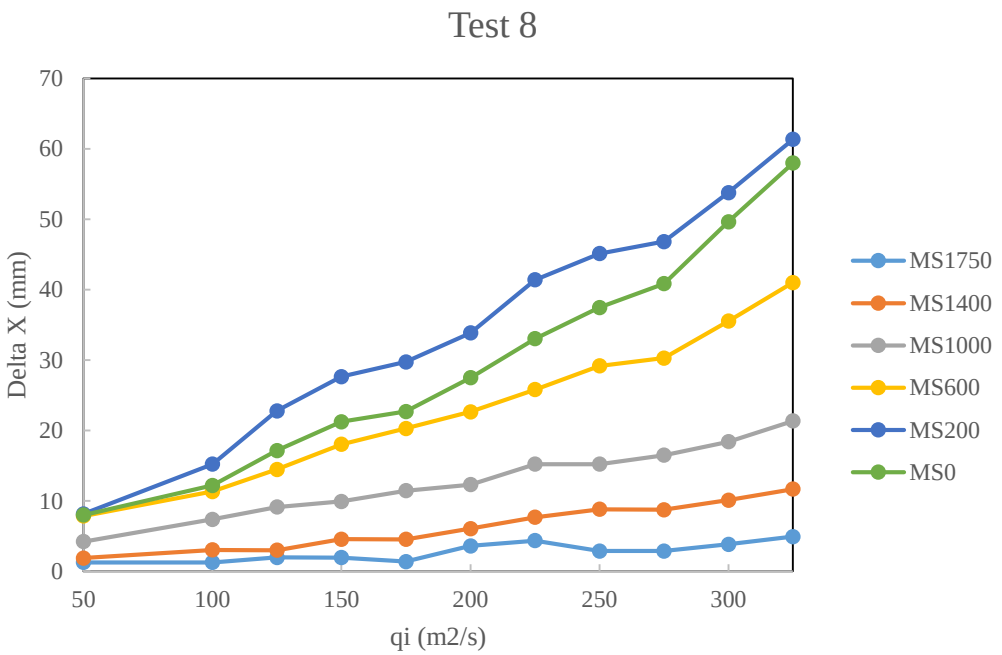

Graph of x-direction displacements with increase in discharge.

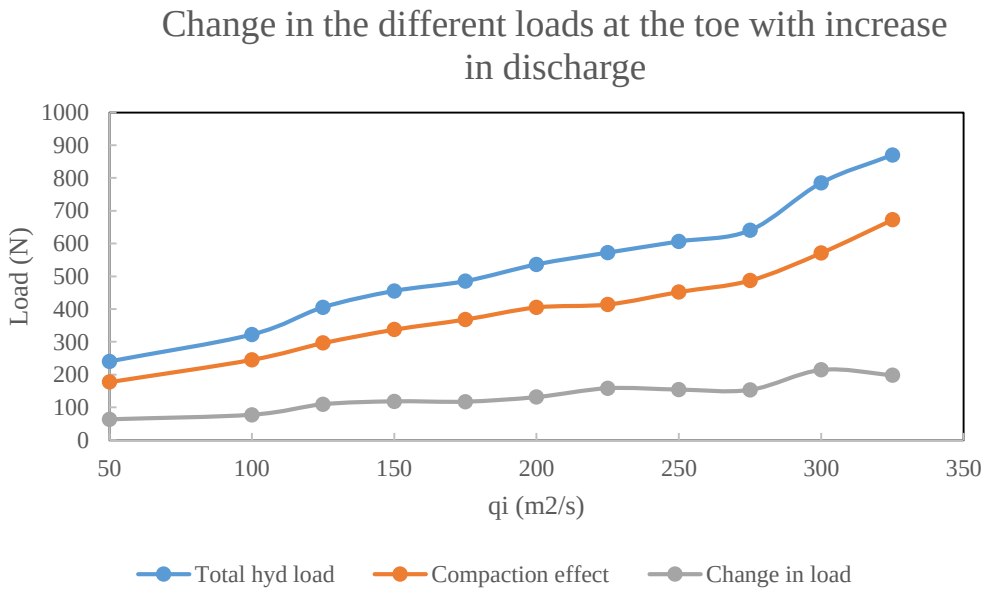

Change in the different loads with change in the discharge which shows stabilization of the load difference after around 150 m2/s.

APPENDIX 8: TEST 9

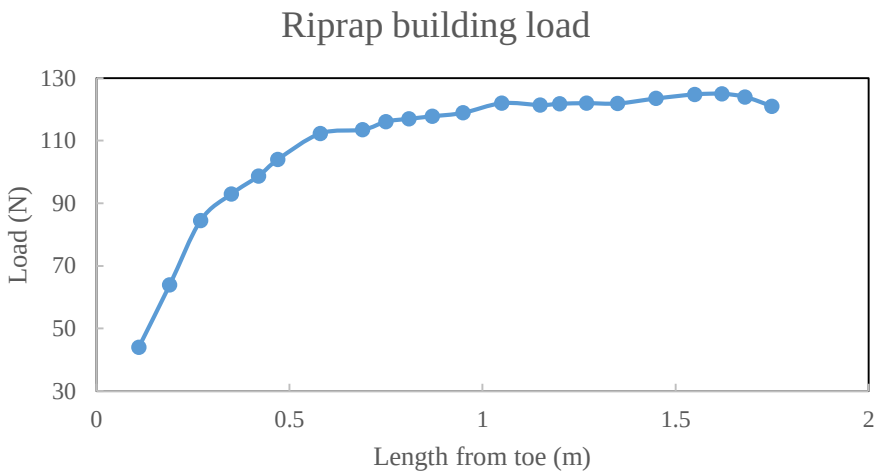

Effect of riprap stone self-weight at the toe of the riprap during riprap construction.

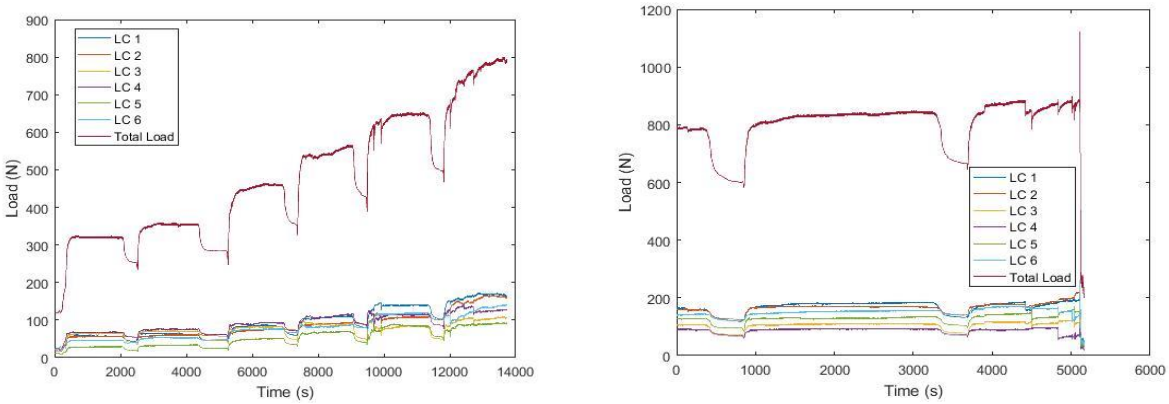

Load profile for test 9 as recorded by the load cells during overtopping test.

Table showing loading values for all incremental discharges during overtopping test for test 9.

q_i (m^2/s)	Total load (N)	Relief Load (N)	THL (N)	Comp. Effect (N)	Load change (N)
0	120				
60	321	253.5	201	133.5	67.5
75	356	283.5	236	163.5	72.5
100	461	354	341	234	107
125	562	427	442	307	135
150	649	496	529	376	153
175	786	600	666	480	186
200	844	665	724	545	179
	880				

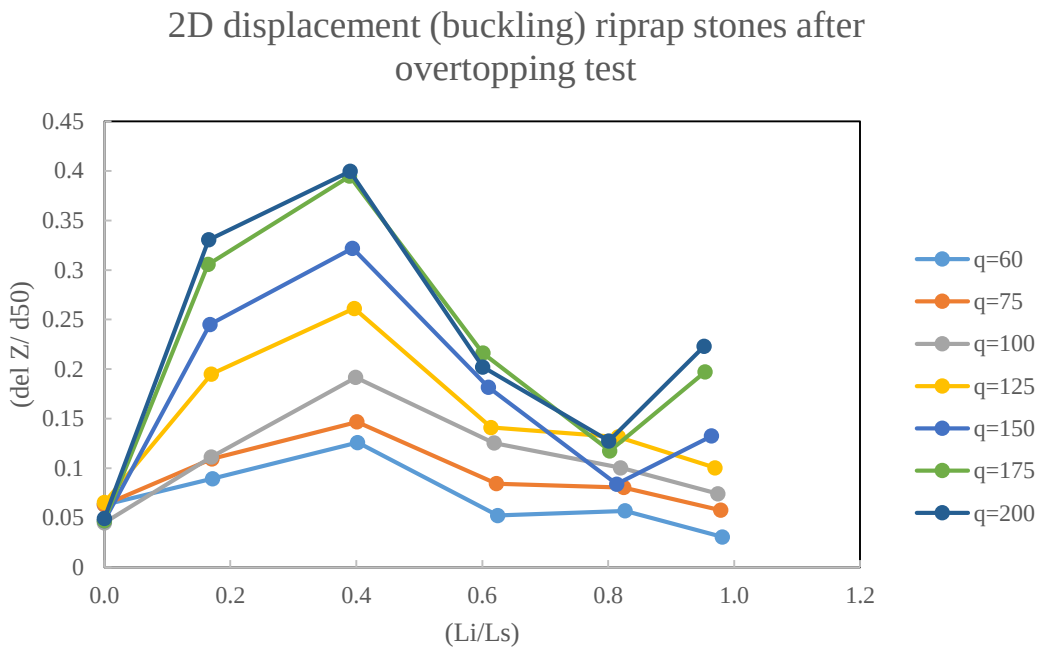

Buckling pattern of marked riprap stones during overtopping test.

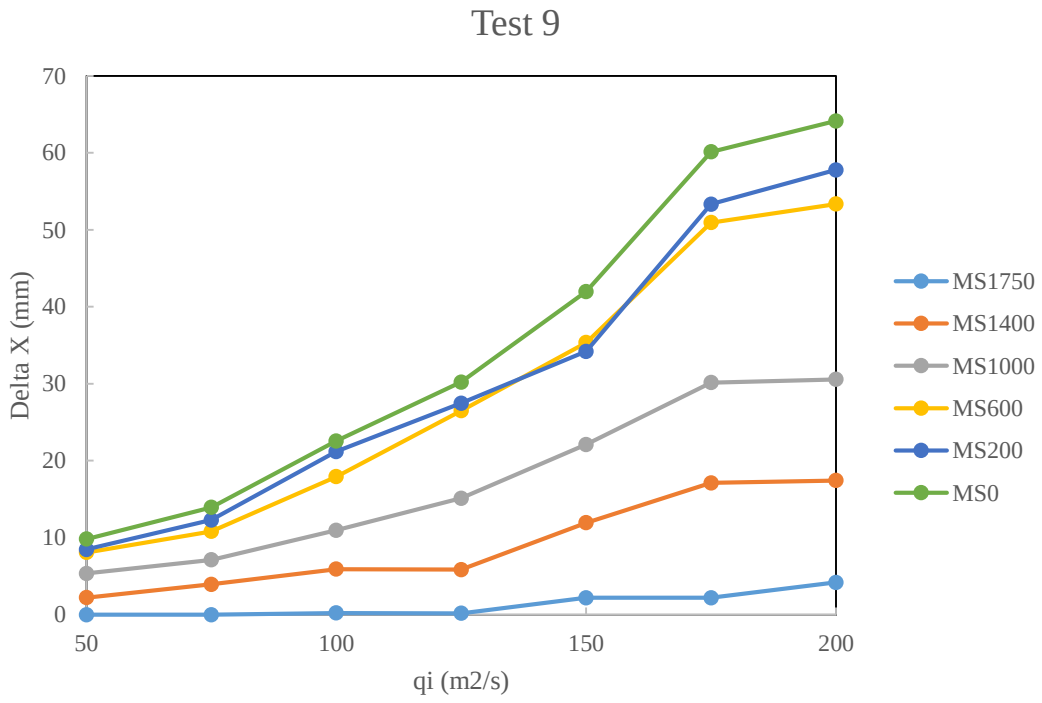

Graph of x-direction displacements with increase in discharge.

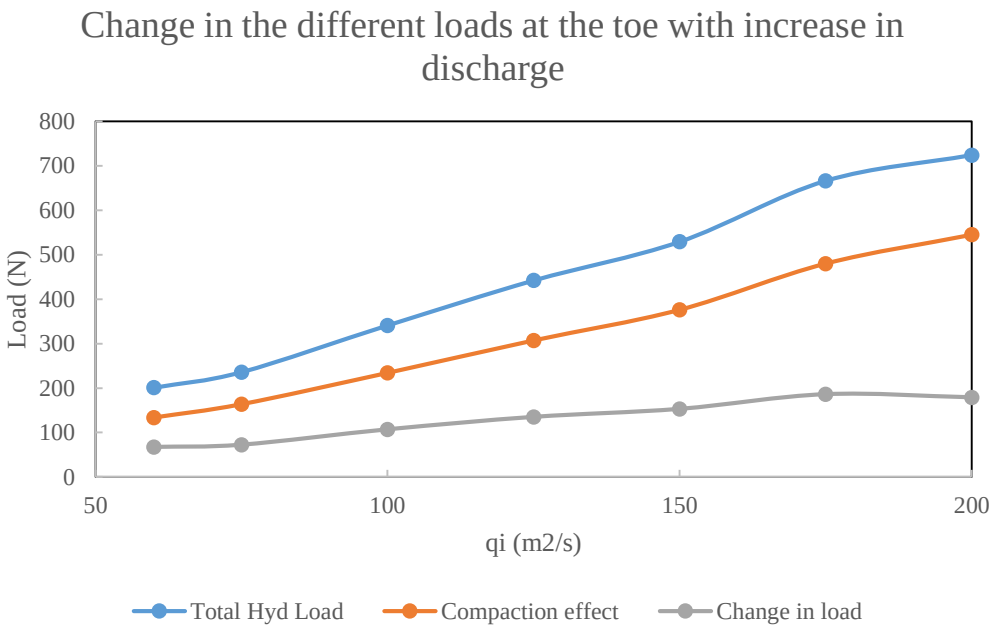

Change in the different load with change in the discharge observed during overtopping test 9.

APPENDIX 9: TEST 10

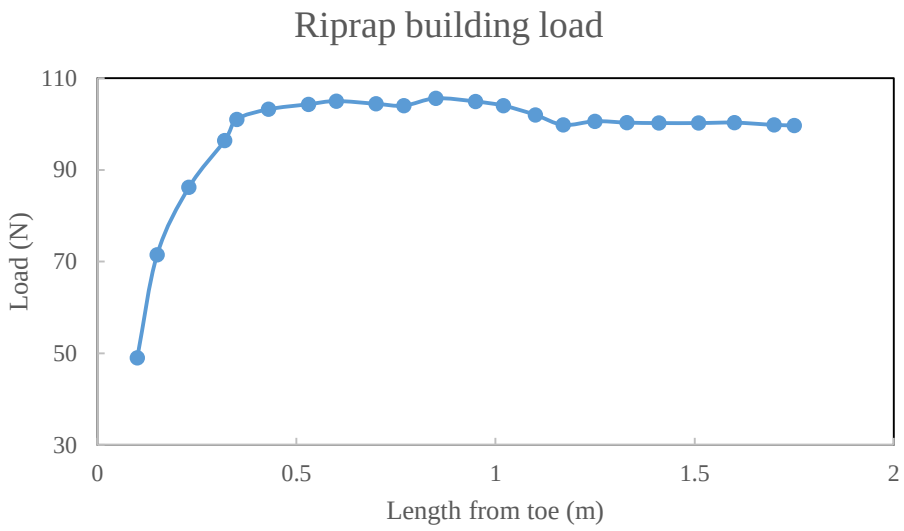

Effect of riprap stone self-weight at the toe of the riprap during riprap construction.

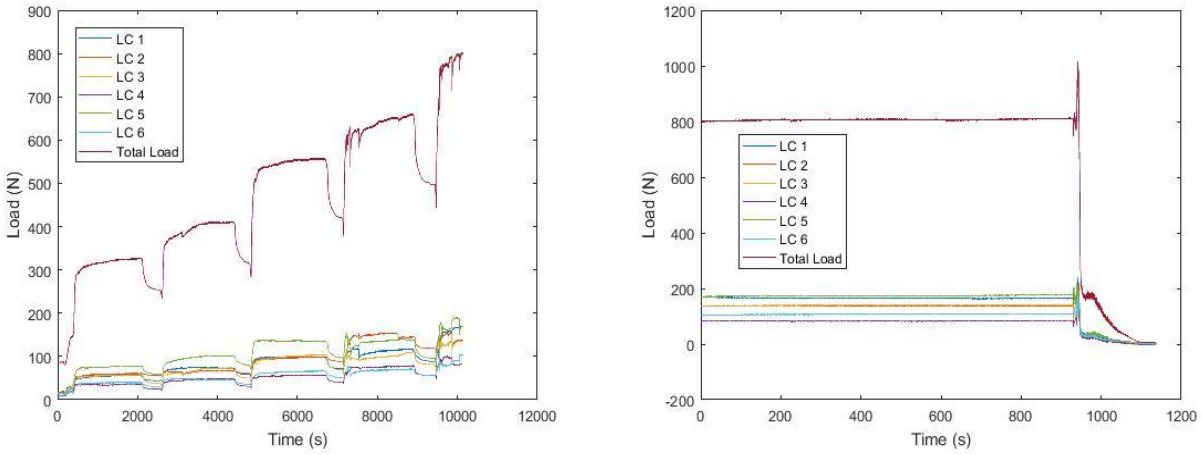

Load profile for test 10 as recorded by the load cells during overtopping test.

Table showing loading values for all incremental discharges during overtopping test 10.

q_i (m^2/s)	Total load (N)	Relief Load (N)	THL (N)	Comp. Effect (N)	Load change (N)
0	100				
50	326	253	226	153	73
75	409	315	309	215	94
100	556	420	456	320	136
125	659	497	559	397	162
	807				

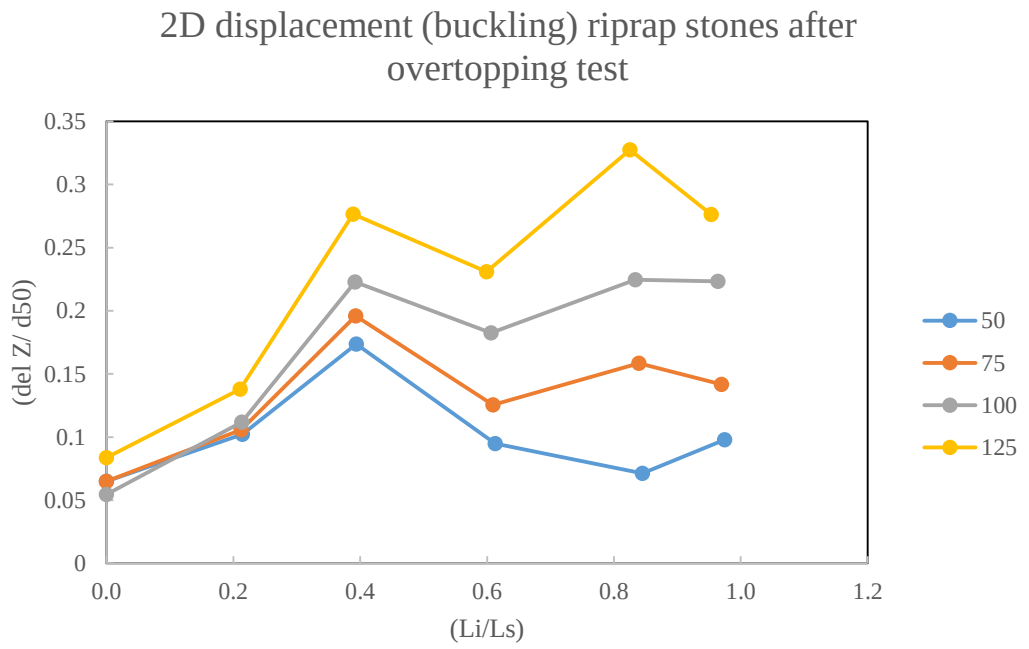

Buckling pattern for marked stones during overtopping test 10.

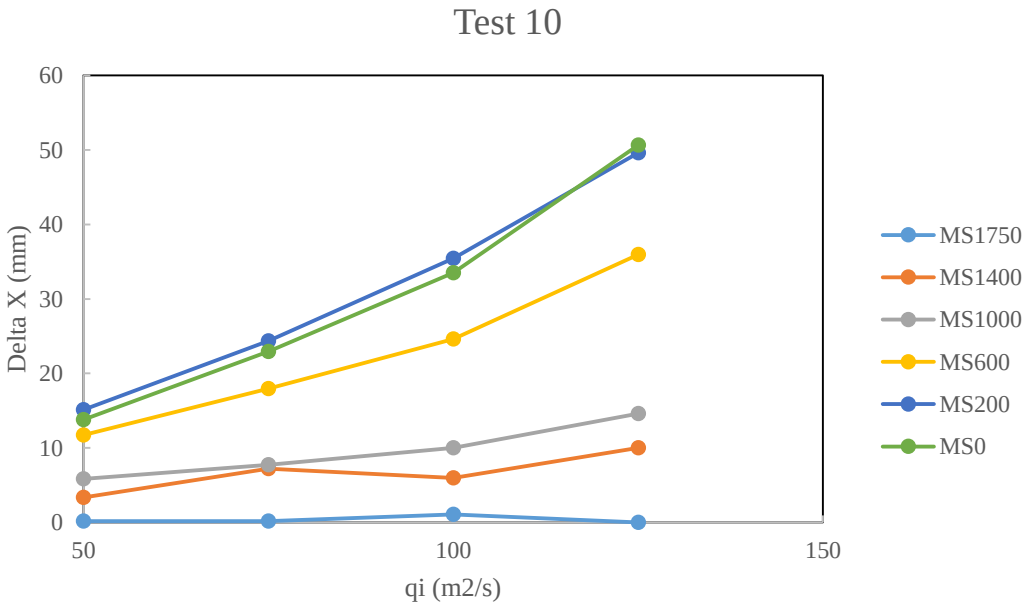

Graph of x-direction displacements with increase in discharge.

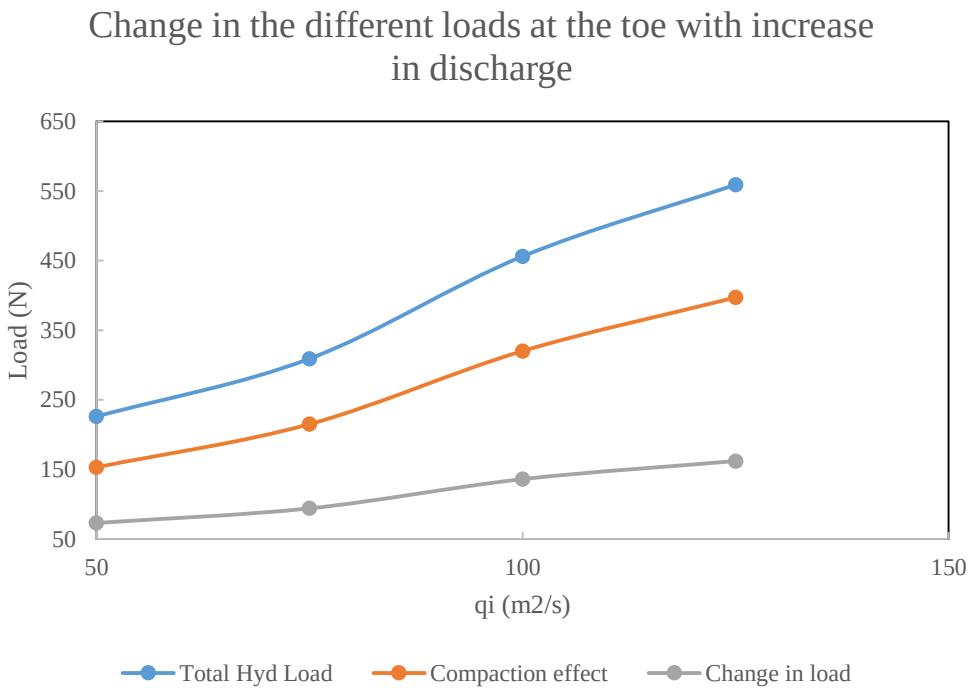

Change in the different loads with change in discharge for overtopping test 10.

APPENDIX 10: RIPRAP STONE MEASUREMENTS

No	a	b	c	Weight	d50
1	93	44	38	270	53.8
2	87	58	23	225	48.8
3	77	48	46	273	55.4
4	95	50	41	203	58.0
5	89	52	39	208	56.5
6	69	40	35	141	45.9
7	92	36	35	121	48.8
8	80	64	42	179	59.9
9	79	36	28	134	43.0
10	84	42	35	185	49.8
11	85	43	32	259	48.9
12	94	52	37	316	56.6
13	84	60	27	187	51.4
14	99	54	46	253	62.7
15	96	45	34	197	52.8
16	91	61	42	255	61.5
17	77	54	42	242	55.9
18	88	51	45	220	58.7
19	84	41	32	160	47.9
20	69	41	39	160	48.0
21	70	58	34	143	51.7
22	90	39	27	139	45.6
23	79	47	44	190	54.7
24	92	43	38	225	53.2
25	80	52	36	188	53.1
26	84	54	35	164	54.1
27	85	45	35	187	51.2
28	96	39	39	170	52.7
29	80	42	32	121	47.6
30	80	41	40	163	50.8
31	90	45	36	157	52.6
32	80	42	29	138	46.0
33	87	67	49	338	65.9
34	76	43	38	144	49.9
35	87	42	23	146	43.8
36	78	49	42	144	54.3
37	88	50	37	192	54.6
38	90	40	30	134	47.6
39	95	42	25	150	46.4
40	84	61	40	210	59.0
41	92	51	31	213	52.6
42	81	41	36	170	49.3
43	95	62	44	220	63.8
44	89	65	38	225	60.4
45	99	46	42	236	57.6
46	84	55	35	207	54.5
47	92	39	35	166	50.1
48	85	26	25	121	38.1
49	95	48	36	250	54.8
50	92	53	51	290	62.9
51	80	57	32	175	52.6
52	85	51	35	221	53.3
53	90	55	43	227	59.7
54	88	46	28	132	48.4
55	97	43	24	128	46.4
56	73	45	40	238	50.8
57	96	46	33	203	52.6
58	76	48	47	251	55.6
59	88	59	48	280	62.9
60	84	56	33	156	53.7
61	80	40	27	135	44.2
62	85	45	30	154	48.6
63	99	53	45	278	61.8
64	76	36	25	102	40.9
65	93	49	45	215	59.0
66	97	56	38	257	59.1
67	85	37	35	143	47.9
68	86	55	40	213	57.4
69	95	47	31	176	51.7
70	75	35	33	115	44.2
71	90	49	30	160	51.0
72	87	43	30	135	48.2
73	98	46	40	234	56.5
74	92	47	44	230	57.5
75	74	51	29	104	47.8
76	83	56	45	221	59.4
77	94	55	46	255	62.0
78	92	33	25	131	42.3
79	78	46	40	204	52.4
80	88	45	44	186	55.9
81	84	39	35	144	48.6
82	85	44	43	209	54.4
83	80	50	35	147	51.9
84	86	56	35	184	55.2
85	76	51	46	270	56.3
86	85	48	46	243	57.3
87	93	55	30	203	53.5
88	81	45	26	134	45.6
89	98	39	36	154	51.6
90	92	44	29	162	49.0
91	85	49	39	255	54.6
92	85	42	34	213	49.5
93	95	41	34	238	51.0
94	81	41	36	204	49.3
95	90	68	34	232	59.3
96	98	55	33	236	56.2
97	74	47	28	143	46.0
98	81	54	39	242	55.5
99	90	55	41	317	58.8
100	92	50	38	326	55.9
101	92	54	40	270	58.4
102	85	54	36	190	54.9
103	77	46	29	126	46.8
104	76	51	31	156	49.3
105	65	43	26	148	41.7
106	82	35	33	150	45.6
107	85	46	29	167	48.4
108	79	47	37	169	51.6
109	90	41	34	178	50.1
110	93	54	45	281	60.9
111	86	40	30	152	46.9
112	92	56	43	351	60.5
113	94	54	30	227	53.4
114	77	56	33	145	52.2
115	98	47	44	258	58.7
116	84	51	35	167	53.1
117	105	65	40	327	64.9
118	92	50	33	205	53.3
119	90	44	37	163	52.7
120	88	41	24	114	44.2
121	91	50	30	130	51.5
122	95	54	32	220	54.8
123	95	47	45	245	58.6
124	85	60	38	257	57.9
125	92	58	47	247	63.1
126	96	48	37	346	55.5
127	92	40	24	170	44.5
128	87	47	20	116	43.4
129	80	47	44	162	54.9
130	75	52	42	183	54.7
131	95	42	40	202	54.2
132	95	54	40	244	59.0
133	100	49	39	212	57.6
134	92	47	28	194	49.5
135	95	55	28	204	52.7
136	84	55	21	200	46.0
137	89	45	42	228	55.2
138	82	51	39	180	54.6
139	80	46	44	212	54.5
140	95	50	42	260	58.4
141	79	53	44	193	56.9
142	90	49	44	206	57.9
143	92	38	33	140	48.7
144	84	47	26	148	46.8
145	85	55	31	150	52.5
146	84	38	34	155	47.7
147	80	55	37	218	54.6
148	89	45	36	210	52.4
149	77	50	35	156	51.3
150	91	40	35	148	50.3
151	95	50	45	296	59.8
152	78	31	25	125	39.2
153	78	56	30	182	50.8
154	95	47	31	174	51.7
155	85	62	43	292	61.0
156	92	35	34	176	47.8
157	78	60	31	182	52.5
158	90	39	34	153	49.2
159	82	44	38	222	51.6
160	90	60	33	199	56.3
161	85	47	38	277	53.3
162	84	56	43	244	58.7
163	80	47	31	158	48.8
164	88	45	36	203	52.2
165	86	55	31	158	52.7
166	94	59	41	227	61.0
167	85	60	42	247	59.8
168	95	42	36	181	52.4
169	88	61	44	310	61.8
170	97	45	40	257	55.9
171	86	42	40	156	52.5
172	84	42	40	153	52.1
173	88	50	28	93	49.8
174	84	49	35	202	52.4
175	79	43	37	176	50.1
176	79	58	45	295	59.1
177	78	48	24	127	44.8
178	85	54	31	252	52.2
179	75	55	36	191	53.0
180	80	55	31	201	51.5
181	97	56	46	375	63.0
182	81	52	40	174	55.2
183	92	45	40	246	54.9
184	85	51	28	147	49.5
185	83	51	49	285	59.2
186	72	48	51	167	56.1
187	79	40	35	161	48.0
188	92	54	30	233	53.0
189	88	55	45	296	60.2
190	96	47	36	190	54.6
191	85	32	29	132	42.9
192	94	54	40	267	58.8
193	100	42	36	185	53.3
194	85	58	44	239	60.1
195	82	50	23	145	45.5
196	75	35	28	118	41.9
197	96	52	32	166	54.3
198	95	60	35	230	58.4
199	99	36	32	217	48.5
200	95	50	31	187	52.8
201	69	55	40	206	53.3
202	70	45	30	194	45.5
203	96	41	30	172	49.1
204	105	56	35	229	59.0
205	85	45	29	153	48.0
206	86	38	35	177	48.5
207	84	55	32	190	52.9
208	87	57	51	387	63.2
209	88	35	32	173	46.2
210	84	50	30	166	50.1
211	78	50	45	230	56.0
212	92	40	37	283	51.4
213	70	32	29	112	40.2
214	90	50	46	268	59.2
215	85	52	27	156	49.2
216	88	64	42	295	61.8
217	84	54	32	154	52.6
218	90	55	28	160	51.8
219	94	41	29	160	48.2
220	92	56	40	270	59.1
221	95	47	42	278	57.2
222	80	55	30	163	50.9
223	76	54	30	188	49.7
224	76	39	38	151	48.3
225	80	54	30	164	50.6
226	93	58	28	183	53.3
227	88	45	32	155	50.2
228	82	52	42	209	56.4
229	75	35	34	122	44.7
230	88	44	25	168	45.9
231	86	50	40	229	55.6
232	85	50	37	230	54.0
233	90	48	30	145	50.6
234	85	52	46	280	58.8
235	85	65	43	291	61.9
236	81	60	28	208	51.4
237	90	45	30	208	49.5
238	89	53	40	287	57.4
239	99	69	42	369	66.0
240	91	45	30	239	49.7
241	81	48	40	218	53.8
242	94	41	33	194	50.3
243	96	47	45	236	58.8
244	88	57	26	197	50.7
245	92	38	32	191	48.2
246	92	59	40	315	60.1
247	91	37	31	184	47.1
248	104	41	32	217	51.5
249	95	55	34	179	56.2
250	90	51	35	310	54.4

No	a	b	c	Weight	d50
251	87	64	51	257	65.7
252	94	65	42	276	63.5
253	94	35	31	168	46.7
254	91	57	45	290	61.6
255	93	51	34	199	54.4
256	90	51	35	182	54.4
257	90	51	41	208	57.3
258	85	41	30	161	47.1
259	80	41	35	138	48.6
260	94	64	38	243	61.1
261	90	64	30	199	55.7
262	90	45	37	255	53.1
263	96	52	34	291	55.4
264	80	45	35	148	50.1
265	94	48	36	171	54.6
266	73	55	36	196	52.5
267	96	48	35	180	54.4
268	100	51	37	254	57.4
269	85	48	45	187	56.8
270	93	57	30	190	54.2
271	90	36	28	130	44.9
272	91	54	51	252	63.0
273	92	44	32	235	50.6
274	90	50	44	255	58.3
275	90	43	32	190	49.8
276	88	51	35	242	54.0
277	84	59	22	191	47.8
278	80	51	51	322	59.3
279	92	50	44	354	58.7
280	102	65	39	326	63.7
281	85	52	39	267	55.7
282	101	47	30	190	52.2
283	82	45	42	225	53.7
284	90	50	35	232	54.0
285	85	46	33	176	50.5
286	100	64	37	333	61.9
287	84	51	30	224	50.5
288	82	46	26	157	46.1
289	85	57	40	300	57.9
290	92	55	34	193	55.6
291	92	51	25	195	49.0
292	84	54	35	192	54.1
293	90	60	35	261	57.4
294	92	42	36	241	51.8
295	91	37	30	162	46.6
296	80	45	33	170	49.2
297	86	46	45	203	56.3
298	87	47	39	183	54.2
299	80	59	30	200	52.1
300	93	46	27	185	48.7
301	86	41	38	170	51.2
302	85	45	36	210	51.6
303	80	60	34	229	54.6
304	75	54	31	163	50.1
305	86	56	44	306	59.6
306	87	54	44	214	59.1
307	96	40	35	209	51.2
308	88	56	34	205	55.1
309	88	51	39	210	55.9
310	99	34	32	181	47.6
311	96	47	39	264	56.0
312	96	44	29	147	49.7

No	a	b	c	Weight	d50
313	78	49	37	172	52.1
314	90	48	41	215	56.2
315	92	54	30	209	53.0
316	91	54	35	213	55.6
317	86	48	41	312	55.3
318	82	45	35	206	50.5
319	77	65	30	206	53.2
320	90	53	33	182	54.0
321	84	50	27	160	48.4
322	94	40	32	237	49.4
323	91	44	36	226	52.4
324	78	52	46	243	57.1
325	97	47	34	205	53.7
326	95	59	40	286	60.7
327	88	58	30	210	53.5
328	90	62	34	216	57.5
329	77	44	38	194	50.5
330	81	37	36	203	47.6
331	90	60	41	234	60.5
332	90	44	34	185	51.3
333	87	50	40	250	55.8
334	101	44	40	177	56.2
335	95	54	48	270	62.7
336	87	45	35	182	51.6
337	99	46	27	176	49.7
338	100	56	36	223	58.6
339	99	45	28	171	50.0
340	88	40	32	181	48.3
341	92	54	36	209	56.3
342	85	55	41	248	57.7
343	83	53	35	267	53.6
344	95	64	30	274	56.7
345	85	60	30	197	53.5
346	88	42	32	180	49.1
347	93	57	42	270	60.6
348	97	58	40	233	60.8
349	84	51	31	159	51.0
350	90	50	34	210	53.5
351	94	51	31	273	53.0
352	95	50	34	234	54.5
353	90	56	40	262	58.6
354	90	44	44	208	55.9
355	86	45	43	228	55.0
356	95	46	40	255	55.9
357	86	55	44	314	59.3
358	85	60	45	266	61.2
359	93	56	45	257	61.7
360	95	46	34	168	53.0
361	88	46	28	169	48.4
362	84	64	29	212	53.8
363	92	60	40	301	60.4
364	84	59	51	227	63.2
365	94	53	41	312	58.9
366	82	45	30	180	48.0
367	87	50	48	238	59.3
368	91	64	38	241	60.5
369	72	50	41	249	52.8
370	92	60	40	304	60.4
371	97	48	30	184	51.9
372	102	39	38	194	53.3
373	92	50	35	228	54.4
374	101	55	35	282	57.9
375	84	50	29	150	49.6

No	a	b	c	Weight	d50
376	86	45	40	162	53.7
377	86	50	45	247	57.8
378	82	46	29	191	47.8
379	88	48	28	160	49.1
380	95	54	49	220	63.1
381	88	38	34	137	48.4
382	80	50	30	153	49.3
383	95	45	35	167	53.1
384	87	54	31	197	52.6
385	82	51	35	182	52.7
386	90	47	28	162	49.1
387	94	45	34	180	52.4
388	78	55	32	176	51.6
389	84	61	49	192	63.1
390	90	52	47	266	60.4
391	100	55	25	249	51.6
392	92	47	46	268	58.4
393	100	49	41	269	58.6
394	80	52	29	136	49.4
395	97	57	40	208	60.5
396	90	50	30	213	51.3
397	80	65	42	302	60.2
398	96	40	31	193	49.2
399	85	36	25	121	42.5
400	104	39	35	218	52.2
401	92	65	44	258	64.1
402	96	42	35	216	52.1
403	97	54	50	275	64.0
404	76	45	42	202	52.4
405	85	55	33	191	53.6
406	93	50	28	231	50.7
407	94	38	30	164	47.5
408	92	49	38	230	55.5
409	87	46	45	266	56.5
410	90	59	44	262	61.6
411	84	50	36	213	53.3
412	93	58	38	227	59.0
413	93	48	45	270	58.6
414	86	50	35	141	53.2
415	98	45	35	173	53.6
416	87	60	44	291	61.2
417	89	50	30	144	51.1
418	95	44	34	146	52.2
419	84	41	34	116	48.9
420	90	38	33	112	48.3
421	79	51	34	124	51.5
422	84	47	38	143	53.1
423	89	46	32	155	50.8
424	103	48	33	178	54.6
425	80	52	45	166	57.2
426	79	51	28	104	48.3
427	93	56	40	234	59.3
428	80	53	34	145	52.4
429	80	44	41	194	52.5
430	103	38	35	133	51.6
431	93	42	31	114	49.5
432	90	42	39	172	52.8
433	96	39	30	133	48.2
434	75	50	36	177	51.3
435	93	59	39	238	59.8
436	83	55	32	156	52.7
437	85	55	45	261	59.5

No	a	b	c	Weight	d50
438	94	51	50	213	62.1
439	78	58	29	155	50.8
440	84	49	36	185	52.9
441	90	51	40	175	56.8
442	80	49	46	268	56.5
443	80	52	26	116	47.6
444	95	45	30	172	50.4
445	88	44	29	144	48.2
446	82	48	47	153	57.0
447	90	46	30	129	49.9
448	80	36	29	114	43.7
449	76	54	50	199	59.0
450	88	46	39	129	54.0
451	75	57	37	269	54.1
452	80	59	35	221	54.9
453	84	54	32	210	52.6
454	79	47	38	183	52.1
455	80	45	25	149	44.8
456	74	57	48	177	58.7
457	99	49	35	259	55.4
458	97	38	34	160	50.0
459	91	49	36	226	54.3
460	84	48	35	214	52.1
461	75	55	36	262	53.0
462	80	57	42	265	57.6
463	94	54	37	212	57.3
464	93	50	41	229	57.6
465	85	35	32	132	45.7
466	90	42	35	215	51.0
467	96	53	29	192	52.8
468	93	54	35	173	56.0
469	90	50	37	235	55.0
470	88	51	36	210	54.5
471	76	38	34	151	46.1
472	92	49	30	175	51.3
473	90	29	29	151	42.3
474	82	52	36	300	53.5
475	80	38	32	147	46.0
476	81	45	34	201	49.9
477	77	47	32	173	48.7
478	86	49	30	265	50.2
479	85	48	35	211	52.3
480	87	58	38	201	57.7
481	89	59	40	258	59.4
482	88	59	48	246	62.9
483	95	38	28	154	46.6
484	88	37	29	139	45.5
485	98	57	32	230	56.3
486	91	46	35	218	52.7
487	80	48	35	226	51.2
488	92	47	37	219	54.3
489	85	46	34	197	51.0
490	105	38	35	240	51.9
491	90	46	46	310	57.5
492	77	47	27	175	46.1
493	100	55	26	202	52.3
494	100	57	36	268	59.0
495	91	35	32	183	46.7
496	84	65	36	230	58.1
497	93	54	37	255	57.1
498	92	46	43	252	56.7
499	81	51	33	193	51.5
500	79	39	29	135	44.7